Journal of Medicinal Chemistry

pubs.acs.org/jmc Article

# Discovery of Arylsulfonamides as Dual Orexin Receptor Agonists

Dehui Zhang, David A. Perrey, Ann M. Decker, Tiffany L. Langston, Vijayakumar Mavanji, Danni L. Harris, Catherine M. Kotz, and Yanan Zhang*

Cite This: J. Med. Chem. 2021, 64, 8806−8825 Read Online

ACCESS | Metrics & More | Article Recommendations | Supporting Information

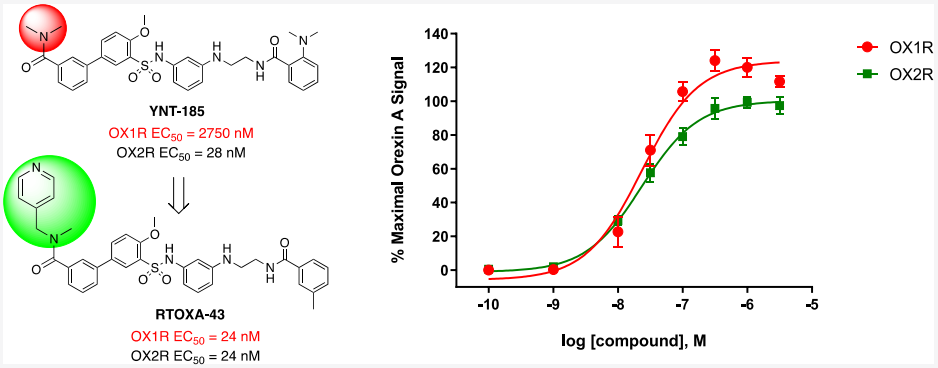


**ABSTRACT:** Loss of orexin-producing neurons results in narcolepsy with cataplexy, and orexin agonists have been shown to increase wakefulness and alleviate narcolepsy symptoms in animal models. Several OX2R agonists have been reported but with little or no activity at OX1R. We conducted structure−activity relationship studies on the OX2R agonist YNT-185 (**2**) and discovered dual agonists such as RTOXA-43 (**40**) with $EC_{50}$'s of 24 nM at both OX2R and OX1R. Computational modeling studies based on the agonist-bound OX2R cryogenic electron microscopy structures showed that **40** bound in the same binding pocket and interactions of the pyridylmethyl group of **40** with OX1R may have contributed to its high OX1R potency. Intraperitoneal injection of **40** increased time awake, decreased time asleep, and increased sleep/wake consolidation in 12-month old mice. This work provides a promising dual small molecule agonist and supports development of orexin agonists as potential treatments for orexin-deficient disorders such as narcolepsy.



## INTRODUCTION

Orexin A and B (also known as hypocretins 1 and 2) are two hypothalamic neuropeptides and the endogenous ligands for two G protein-coupled receptors (GPCRs), orexin-1 (OX1R), and orexin-2 (OX2R).[1,2] Orexin-expressing neurons are limited in number and located predominantly in a small area of the lateral hypothalamus;[2−5] however, the nerve fibers of orexin neurons project throughout the central nervous system and their afferents are sent to many brain regions in cortical, limbic, and brainstem circuits.[3,6−8] The orexin system has been shown to modulate a variety of important behavioral and physiological processes, including sleep/wakefulness,[9,10] arousal,[11,12] feeding,[2] energy homeostasis,[2] stress and anxiety,[13−16] and learning and memory.[17−20]

Loss of orexin-producing neurons results in narcolepsy with cataplexy, an incurable chronic neurological disorder characterized with sleep disruptions (excessive daytime sleepiness, fragmented sleep and intrusions of sleep episodes during the active phase, etc.).[21−24] Narcolepsy affects an estimated 200,000 Americans and approximately 3 million worldwide and severely impacts the day-to-day lives of affected individuals. Central orexin-A administration successfully enhances wakefulness and consolidates sleep/wake states.[25] Consistent with orexin's multifaceted role, orexin deficiency has also been linked to abnormalities in energy homeostasis, stress-related behavior, and reward systems[26] and is believed to be associated with pathophysiologies such as obesity and age-related disorders.[27] A loss of orexin neurons and/or orexin peptides has been found in Alzheimer's and Parkinson's patients,[28−32] as well as in aged humans and mice.[17−19]

Medication development targeting the orexin system has largely focused on antagonists thus far as over- or abnormal activation of the orexin system leads to insomnia.[33,34] A large number of orexin receptor antagonists, dual- or subtype-selective, have been developed.[35−39] Two dual antagonists, suvorexant and more recently lemborexant, have been approved by the FDA for the treatment of insomnia. Orexin

Received: May 9, 2021
Published: June 8, 2021




https://doi.org/10.1021/acs.jmedchem.1c00841
J. Med. Chem. 2021, 64, 8806−8825

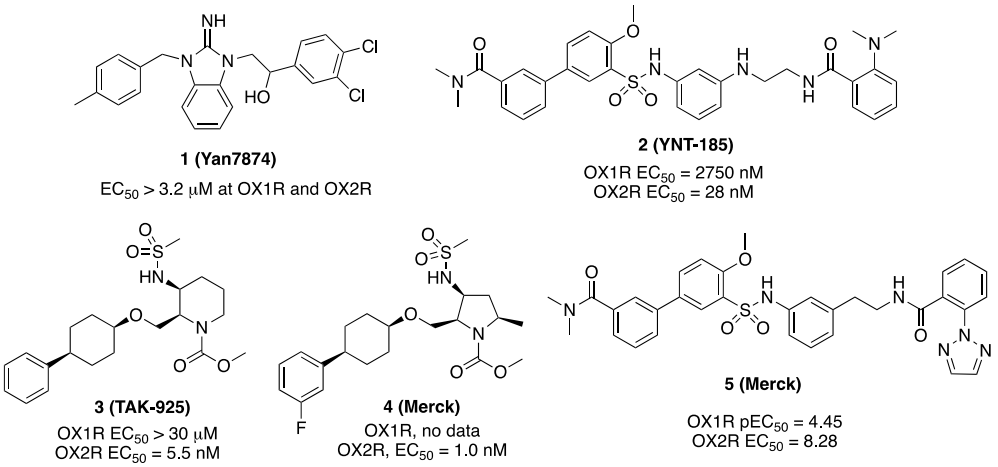


**Figure 1.** Small-molecule orexin agonists reported in the literature.

antagonism has also shown early promises in the treatment of drug addiction and anxiety disorders.[13,14,16,36,40−42] In contrast, activation of the orexin receptors is primarily accomplished using orexin peptides, particularly the more stable orexin-A (33 AA with two disulfide bridges). Only a limited number of small-molecule orexin agonists have been disclosed thus far. Yan7874 (**1**) was first reported as a small-molecule OX2R agonist in a 2010 patent (Figure 1);[43] however, it was later confirmed to be a weak agonist of both OX receptors ($EC_{50}$ > 3.2 $\mu$M) and also showed OX receptor independent cytotoxicity.[44] YNT-185 (**2**) was reported in 2015 and displayed good OX2R potency and selectivity over OX1R ($EC_{50}$ = 28 nM vs 2750 nM at OX1R).[45] Intracerebroventricular (i.c.v., 30−300 nmol) and/or intraperitoneally (i.p., 40 mg/kg) administration of **2** (hydrochloride salt) promoted wakefulness without affecting body temperature in wild-type mice, whereas in orexin knock-out (KO) and orexin neuron-ablated mice, **2** suppressed cataplexy-like episodes.[46] In another study, **2** attenuated morphine-induced sedative effects in rats, as assessed by electroencephalogram (EEG) changes and behavioral measures including locomotor activity and startle response latency, without affecting the analgesic effect of morphine.[47] More recently, a series of substituted piperidines as OX2R agonists was reported, and Tak-925 (**3**) is currently in phase 1 clinical trials for the treatment of narcolepsy.[48] Another small-molecule orexin agonist by Takeda, TAK-994, is in a phase 2 clinical trial in type 1 and 2 narcoleptic patients (www.clinicaltrials.gov), although its structure is not disclosed. A series of structurally similar OX2R agonists based on a pyrrolidine core (e.g., **4**) were reported in 2020 with high potencies at OX2R, but no data were reported on OX1R activity.[49] Finally, the cryogenic electron microscopy (cryo-EM) structure of the first agonist-bound OX2R using agonist **5** was recently reported, providing structural insights for agonist−receptor interactions.[50]

The two orexin receptors (and their mRNAs) have overlapping, but sometimes distinct, patterns of distribution in the brain,[3,5,51,52] suggesting that they may play differential physiological roles. For instance, mice lacking OX2R display several abnormalities similar to human narcolepsy;[18,53] however, the behavioral phenotype of OX2R KO mice appears less severe than orexin null mice, and double-orexin-receptor KO mice displayed sleep/wake disturbances most similar to human narcolepsy.[54−56] Similarly, although OX2R antagonists were shown to be efficacious in promoting sleep,[57] a number of preclinical studies have suggested that antagonizing both orexin receptors was more effective.[54,58,59] Given the role of the OX1R in many functions and the equal potency of the endogenous peptide orexin-A, agonists that also have OX1R activity are desired. We conducted structure−activity relationship (SAR) studies on **2** with structural modifications at several sites (Figure 2) and developed a series of new orexin agonists

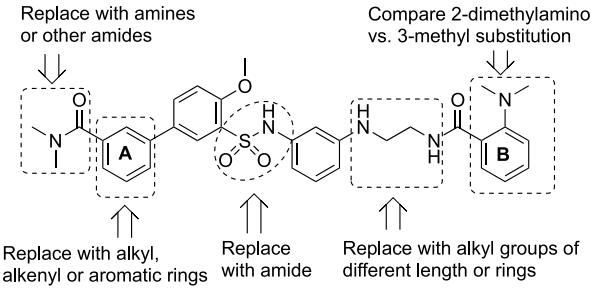


**Figure 2.** SAR strategies on **2**.

(**6**−**44**). One of the most potent compounds (RTOXA-43, **40**) showed good potencies at both OX1R and OX2R ($EC_{50}$ = 24 at both OX1R and OX2R) when evaluated in calcium mobilization assays using cells overexpressing these receptors. Excitingly, **40** (40 mg/kg, i.p.) increased time awake, decreased time asleep, and increased sleep/wake consolidation when measured using continuous EEG/electromyogram (EMG) recordings in 12-month-old mice. Hereby, we describe the design, synthesis, and pharmacological characterization of these orexin receptor agonists.

## RESULTS AND DISCUSSION

**Chemistry.** The syntheses of all target compounds were accomplished following procedures shown in Schemes 1−6. Compounds **2** and **6**−**16** with modifications on ring-A were synthesized following the procedures described by Nagahara and co-workers.[45] Commercially available 1-fluoro-3-nitrobenzene was reacted with excess ethylenediamine at 120 °C for 12 h to afford the substituted aniline, which was immediately reacted with $Boc_2O$ to give **45** in 63% over two steps. The aniline group in **45** was then protected by treatment with benzyl bromide in the presence of potassium carbonate in dimethylformamide (DMF) to afford the key intermediate **46**


https://doi.org/10.1021/acs.jmedchem.1c00841
J. Med. Chem. 2021, 64, 8806−8825

**Scheme 1. Syntheses of Compounds 2 and 6−16**[a]

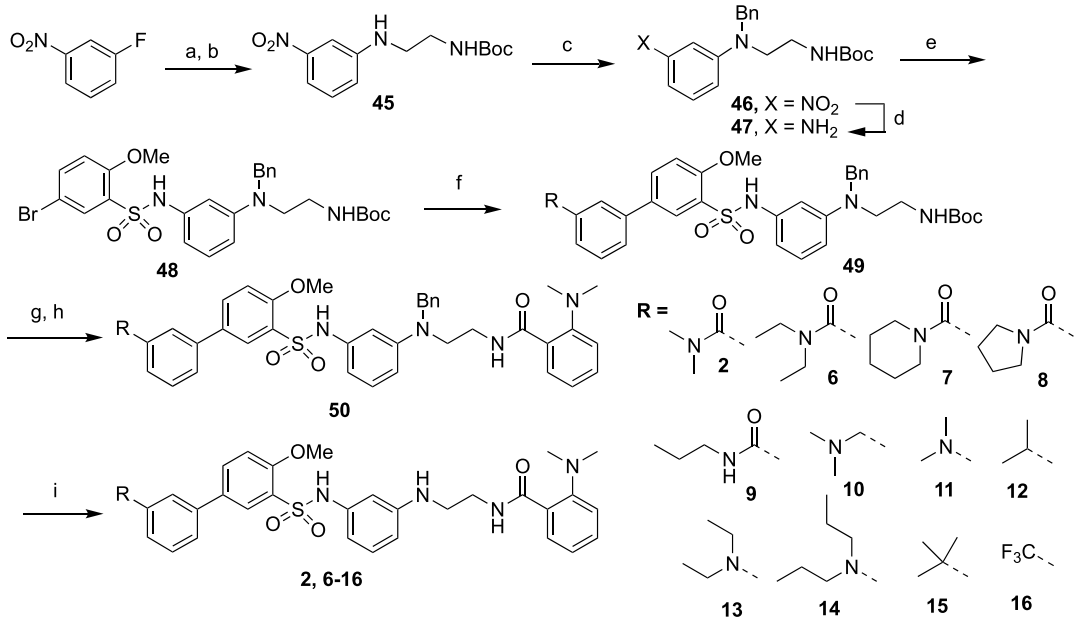


[a]Reagents and conditions: (a) ethylenediamine, 120 °C, sealed tube, overnight; (b) $Boc_2O$, $K_2CO_3$, THF/$H_2O$, 63% over two steps; (c) BnBr, $K_2CO_3$, DMF, 60 °C, 62%; (d) Fe, $NH_4Cl$, EtOH, reflux, 98%; (e) 2-methoxy-5-bromobenzenesulfonyl chloride, pyridine, DCM, 0 °C to rt, 90% (f) boronic acid, $Pd(PPh_3)_4$, $K_2CO_3$, 1,4-dioxane/$H_2O$ (4:1), 90 °C; (g) 4 N HCl in 1,4-dioxane; (h) 2-dimethylamino benzoic acid, HATU, DIPEA, DMF; (i) $H_2$, Pd/C, MeOH, 29−45% over four steps.

**Scheme 2. Syntheses of Compounds 17−21**[a]

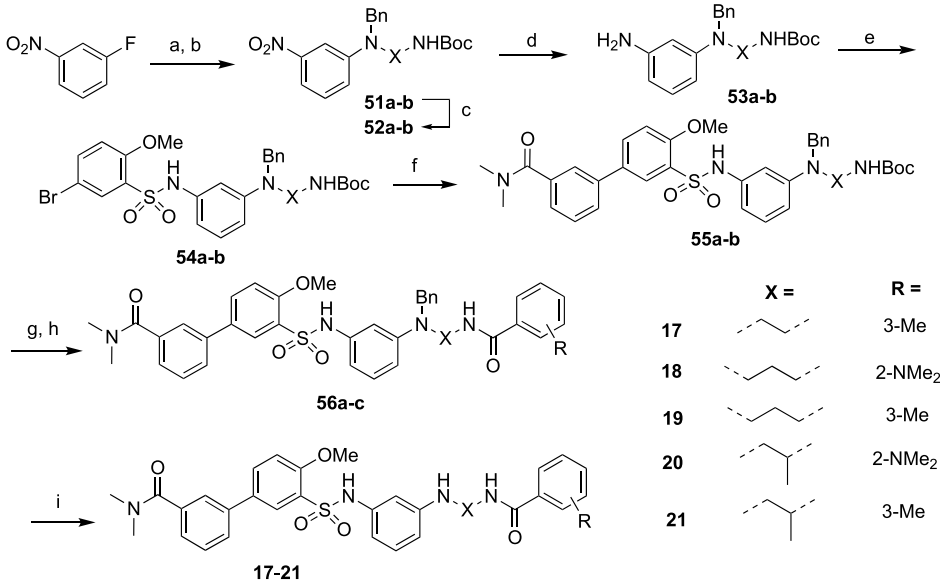


[a]Reagents and conditions: (a) appropriate diamine, 120 °C, sealed tube, overnight; (b) $Boc_2O$, $K_2CO_3$, THF/$H_2O$, 72% for **51a**, 30% for **51b** over two steps; (c) BnBr, $K_2CO_3$, DMF, 60 °C, 84% for, **52a**, 81% for **52b**; (d) Fe, $NH_4Cl$, EtOH, reflux, 92% for **53a**, 92% for **53b**; (e) 2-methoxy-5-bromobenzenesulfonyl chloride, pyridine, DCM, 0 °C to rt, 85% for **54a**, 83% for **54b**; (f) *N*,*N*-dimethylbenzamide-3-boronic acid, $Pd(PPh_3)_4$, $K_2CO_3$, 1,4-dioxane/$H_2O$ (4:1), 90 °C; (g) 4 N HCl in 1,4-dioxane; (h) substituted benzoic acid, HATU, DIPEA, DMF; (i) $H_2$, Pd/C, MeOH, 19−32% over our steps.

in 62% yield. Reduction of the nitro group using iron gave amine **47** almost quantitatively (98%). Reaction of 5-bromo-2-methoxybenzenesulfonyl chloride in tetrahydrofuran (THF) with **47** in dichloromethane (DCM) in the presence of pyridine led to intermediate **48** in excellent yield (90%). Suzuki coupling of **48** with different boronic acids gave intermediate **49**, which was immediately submitted to acidic Boc deprotection and amide coupling to provide **50**. Finally, deprotection of the benzyl group of **50** using hydrogenation catalyzed by palladium on carbon afforded target products **2** and **6−16** in 29−45% yield over four steps.

Similarly, compounds **17** to **21** that examine the importance of the ethyl linker were synthesized following a similar sequence, as shown in Scheme 2, using different diamines


https://doi.org/10.1021/acs.jmedchem.1c00841
J. Med. Chem. 2021, 64, 8806−8825

**Scheme 3. Syntheses of Compounds 22 and 23**[a]

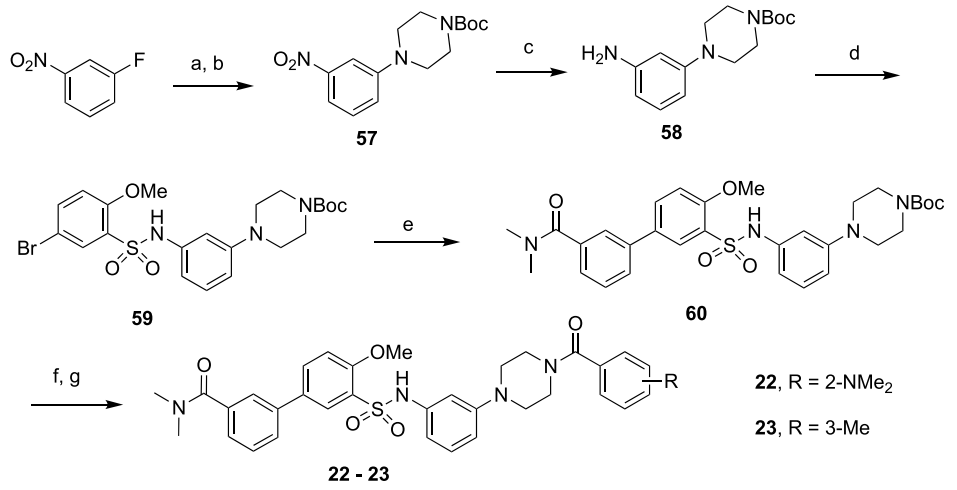


[a](a) Piperazine, 100 °C, sealed tube,overnight; (b) $Boc_2O$, $K_2CO_3$, THF/$H_2O$, 49% over two steps; (c) Fe, $NH_4Cl$, EtOH/$H_2O$, reflux, 86%; (d) 2-methoxy-5-bromobenzenesulfonyl chloride, pyridine, DCM, 0 °C to rt, 80%; (e) *N*,*N*-dimethylbenzamide-3-boronic acid, $Pd(PPh_3)_4$, $K_2CO_3$, 1,4-dioxane/$H_2O$ (4:1), 90 °C; (f) 4 N HCl in 1,4-dioxane; (g) substituted benzoic acid, HATU, DIPEA, DMF, 36% for 22, 41% for 23 over three steps.

**Scheme 4. Synthetic Route to Compounds 24−32**[a]

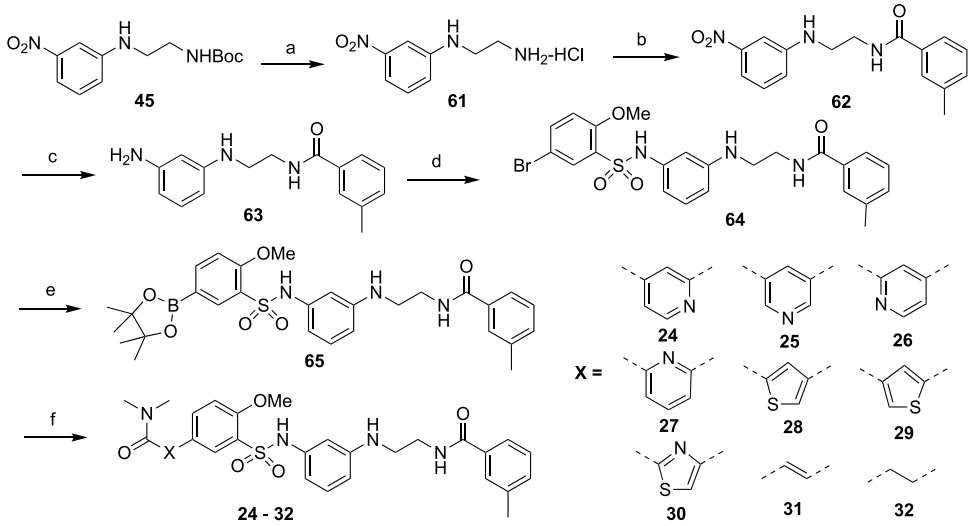


[a]Reagents and conditions: (a) 4 N HCl in 1,4-dioxane, 78%; (b) 3-methyl benzoic acid, HATU, DIPEA, DMF; (c) Fe, $NH_4Cl$, EtOH, reflux, 62% over three steps; (d) 2-methoxy-5-bromobenzenesulfonyl chloride, $NEt_3$, $DMAP_{(cat.)}$, DCM/THF, 0 °C to rt, 76%; (e) $B_2pin_2$, $PdCl_2dppf$, KOAc, 1,4-dioxane, 90 °C, 87%; (f) R−Br or R−I, $Pd(PPh_3)_4$, $K_2CO_3$, 1,4-dioxane/$H_2O$ (4:1), 63−88%.

**Scheme 5. Synthesis of Compounds 33−42**[a]

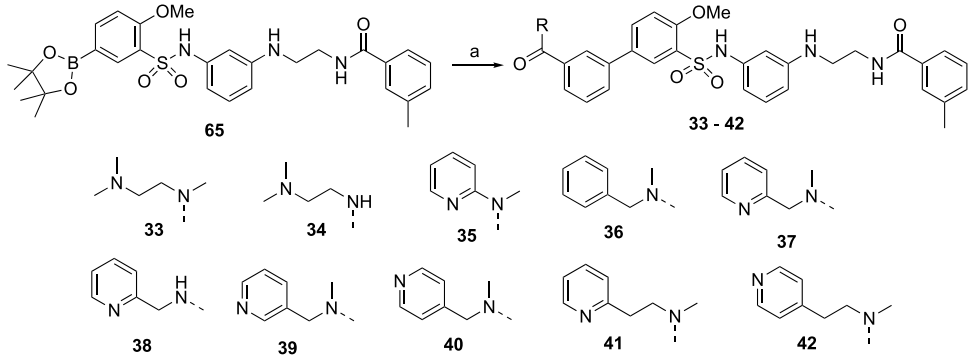


[a]Reagents and conditions: (a) aryl halide, $Pd(PPh_3)_4$, $K_2CO_3$, 1,4-dioxane, $H_2O$, 62−85%.



https://doi.org/10.1021/acs.jmedchem.1c00841
J. Med. Chem. 2021, 64, 8806−8825

**Scheme 6. Synthesis of Compounds 43 and 44**[a]

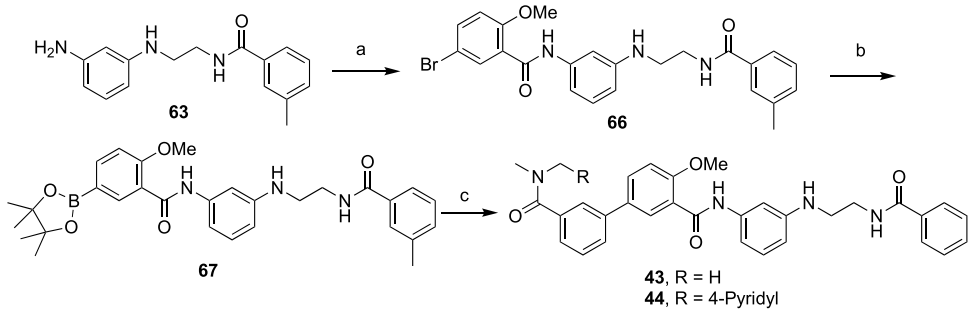


[a]Reagents and conditions: (a) 2-methoxy-5-bromobenzenecarboxylic chloride, $NEt_3$, DIPEA, DCM, 0 °C to rt, 60%; (b) $B_2pin_2$, $PdCl_2dppf$, KOAc, 1,4-dioxane, 90 °C, >99%, (c) aryl halide, $Pd(PPh_3)_4$, $K_2CO_3$, 1,4-dioxane/$H_2O$ (4:1), 78% for **43**, 72% for **44**.

instead of ethylenediamine. 1-Fluoro-3-nitrobenzene underwent fluoro displacement with diamines, Boc protection, and benzyl protection to give **52**, which was then reduced to give amine **53** in excellent yield (92%). Coupling of **53** with 5-bromo-2-methoxybenzenesulfonyl chloride afforded **54**, which was subjected to Suzuki coupling to give intermediate **55**. Boc deprotection followed by amide coupling furnished **56**, deprotection of which provided final compounds **17**−**21** in 19−32% yield over four steps.

For compounds **22** and **23** with a piperidine group, since the protection of nitrogen was not needed, a simplified synthetic route was followed (Scheme 3). 1-Fluoro-3-nitrobenzene was reacted with excess piperazine followed by Boc protection to give **57** in 49% yield. Reduction of the nitro group provided amine **58**, which was then reacted with 5-bromo-2-methoxybenzenesulfonyl chloride to afford **59** in 80% yield. Suzuki coupling furnished **60**, followed by Boc deprotection and amide coupling to give final compounds **22**−**23** in 36 and 41% yields, respectively, over three steps.

Compounds **24**−**32**, in which ring-A was replaced with other aromatic or alkyl groups, were synthesized following modified procedures as shown in Scheme 4. In order to facilitate the examination of the SAR on the left-hand side, the amide on the right was installed first. In addition, to simplify the synthetic route, we attempted to not protect the aniline using a benzyl group as previously described but to install the sulfonamide selectively at the more accessible primary amino group. Thus, **45** was treated with 4 N HCl in dioxane to afford the amine **61**. Amide coupling between compound **61** and 3-methylbenzoic acid led to **62**, which was reduced using iron to give **63** in 62% over two steps. Slow addition of a diluted solution of 5-bromo-2-methoxybenzenesulfonyl chloride in THF into a diluted solution of **63** in DCM in the presence of triethylamine and catalytic 4-dimethylaminopyridine (DMAP) at 0 °C afforded **64** in 76% yield, with the selective acylation of the less hindered amino groups. This sequence avoided the protection/deprotection steps and afforded the desired product in good yields. The subsequent Miyaura borylation reaction gave boronic acid pinacol ester **65**, which was readily reacted with different aromatic bromides or iodides to furnish the final products **24**−**32** in 63−88% yield.

Compounds **33**−**42** with different amide functionalities on ring-A were prepared in good yields following a Suzuki coupling of intermediate **63** with the appropriate aryl halides under standard conditions in 62−85% yield.

Amide coupling between intermediate **63** and 5-bromo-2-methoxybenzoic acid chloride afforded bromide **66** in 60% yield. Miyaura borylation of **66** using bis(pinacolato)diboron provided **67** quantitatively, which then underwent a Suzuki coupling reaction with the halides to provide compounds **43** and **44** in good yield (78 and 72%, respectively). In these two compounds, the sulfonamide was replaced with an amide functionality.

**Potency in OX1R and OX2R Calcium Mobilization Assays.** All target compounds were evaluated for their agonist potencies in calcium mobilization assays using CHO RD-HGA16 cells (Molecular Devices) engineered to stably express either the human OX2R or OX1R as previously described.[60] In this assay platform, receptor activation is measured by an increase in fluorescence, which is directly proportional to an increase in internal calcium. The $EC_{50}$ values are listed in Tables 1−5. YNT-185 (**2**) was previously reported to have $EC_{50}$ values of 28 nM at OX2R and 2750 nM at OX1R.[45] However, in our orexin calcium mobilization assays, **2** displayed potencies of 165 and 824 nM at OX2R and OX1R, respectively. The potency differences may have resulted from the differently engineered cell lines. While both groups use calcium mobilization assays to measure receptor activation, Nagahara and colleagues used CHO cells coexpressing the orexin receptors and a luciferase reporter,[45] and our group used $G\alpha_{16}$-expressing CHO cells. In their assays, orexin-A had $EC_{50}$'s = 1.0 and 1.5 nM at OX2R and OX1R, respectively, whereas the $EC_{50}$ values are 0.6 and 0.3 nM in our assays, respectively.

In our SAR studies, we first examined substitutions on aromatic ring-A on the left-hand side of the structure (Table 1). The dimethylamino amide on **2** was replaced with several differently substituted alkyl amides including diethylamino (**6**), cyclic (**7**, **8**), or secondary amides (**9**). However, most of the compounds showed similar or even reduced potencies at OX2R and/or OX1R, with **9** showing no activity at OX1R. We then attempted to remove the carbonyl functionality, which resulted in a decrease in potency at OX2R (**10**, $EC_{50}$ = 560 nM), whereas no activity was observed at OX1R. None of the other amino or alkyl groups (**11**−**16**) showed activity at either receptor. Together, these results confirmed the importance of the carbonyl functionality for orexin receptor activation.

We next examined substitutions on aromatic ring-B on the right-hand side as well as the ethyl linker (Table 2). Consistent with results reported by Nagahara et al.,[45] replacement of the 2-dimethylamino with a 3-methyl group (**17**) slightly improved potencies at both OX2R and OX1R (56 vs 165 nM at OX2R; 326 vs 826 nM at OX1R). Elongation of the ethyl group to the 3-carbon propyl group (**18**−**19**) or addition of a methyl group


https://doi.org/10.1021/acs.jmedchem.1c00841
J. Med. Chem. 2021, 64, 8806−8825

**Table 1**

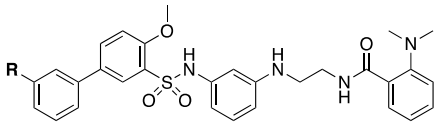

| No. | R | OX1R[a] | | OX2R[a] | | OX1R/ |
|---|---|---|---|---|---|---|
| | | $EC_{50}$ (nM) | $E_{max}$ (%) | $EC_{50}$ (nM) | $E_{max}$ (%) | OX2R |
| **2** |  | 824 ± 56 | 84 ± 2 | 165 ± 43 | 100 ± 2 | 4.99 |
| **6** |  | 737 ± 72 | 90 ± 2 | 222 ± 44 | 103 ± 4 | 3.32 |
| **7** |  | 2430 ± 440 | 55 ± 4[c] | 456 ± 69 | 74 ± 7 | 5.33 |
| **8** |  | 830 ± 107 | 83 ± 5 | 252 ± 50 | 94 ± 4 | 3.29 |
| **9** | 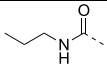 | >10,000[b] | - | 753 ± 150 | 55 ± 8 | >13.2 |
| **10** |  | >10,000[b] | - | 560 ± 160 | 82 ± 6[c] | >17.8 |
| **11** |  | >10,000[b] | - | 2130 ± 240 | 46 ± 6[c] | >4.69 |
| **12** |  | >10,000[b] | - | >10,000[b] | - | - |
| **13** |  | >10,000[b] | - | 4150 ± 770 | 48 ± 2[c] | >2.41 |
| **14** |  | >10,000[b] | - | >10,000[b] | - | - |
| **15** |  | >10,000[b] | - | >10,000[b] | - | - |
| **16** |  | >10,000[b] | - | >10,000[b] | - | - |

[a]$EC_{50}$ and $E_{max}$ values (% of orexin-A control) are the means ± SEM of at least three independent experiments conducted in duplicate. [b]Values are from two independent experiments conducted in duplicate. [c]Concentration−response curve does not have a top plateau.

(**20**−**21**) resulted in little change in potency. However, when the ethyl group was converted to a rigid piperazine group (**22**−**23**), all activities were lost. In general, in this series, the 3-methyl analogues appeared to provide better potencies at OX1R than the corresponding 2-dimethylamino analogues (**2**, **18**, and **20** vs **17**, **19**, and **21**), and we therefore used 3-methylamino in the subsequent SAR studies.

Phenyl ring-A was then replaced with other aromatic rings or a rigid alkenyl or an ethyl group (Table 3). Out of the four pyridine groups (**24**−**27**), the 2,6-substituted pyridine (**27**) afforded the best potencies at both OX1R and OX2R ($EC_{50}$'s = 74 nM at OX2R and 226 nM at OX1R), with $EC_{50}$ values lower than **2**, and appeared to be a full agonist at both OX1R and OX2R. We then investigated several five-membered heteroaromatic rings (**28**−**30**), including thiophenes and a thiazole, and they were similar or less potent than **2** at OX2R, with little activity at OX1R. Interestingly, these five-membered analogues (**28**−**30**) all acted as partial agonists at both OX1R and OX2R. The ethylenyl (**31**) and the ethyl (**32**) analogues, which were designed to provide structural flexibility, were both inactive at both receptors. These results suggest that an aromatic group is preferred at this position.

Given the importance of the carbonyl group of the amide functionality on ring-A, we retained the amide and explored further substitutions at this position (Table 4). First, we replaced one of the methyl groups on the amide with a dimethylaminoethyl group (**33**), which offers a site for salt formation to improve solubility. However, a slight reduction in potency was observed ($EC_{50}$ = 293 nM at OX2R and 638 nM at OX1R). Notably, removal of the other methyl on the nitrogen resulted in a sharp decrease of potency at OX2R (**33** vs **34**) and complete loss of potency at OX1R. This is consistent with earlier observations that primary amides were not favored (**9**). Introduction of a pyridyl (**35**) group in place of a methyl on the dimethylamino group led to a significant decrease in potency at both receptors. Interestingly, while a benzyl (**36**) showed lowered potency at OX2R and no activity at OX1R, 2-pyridylmethyl group (**37**) led to better potencies than **2** at both OX receptors ($EC_{50}$ = 107 nM at OX2R and 235 nM at OX1R). This suggests that hydrogen bonding or polar−polar interaction between the pyridyl group and the OX receptors may be present. Similarly, removal of the other methyl on the dimethylamino group again led to complete loss of the OX1R potency (**38**). Considering the potency enhancement by the pyridyl group, we began to finely tune the substitution and examine different pyridylmethyl groups. While 3-pydidylmethyl (**39**) showed a slight drop in potency ($EC_{50}$ = 134 nM at OX2R; 460 nM at OX1R), excitingly, **40** with a 4-pyridylmethyl group showed high and equal potencies at both OX2R and OX1R ($EC_{50}$ = 24 nM), significantly more potent than **2**. Compound **40** was a full agonist at both OX2R and OX1R, with $E_{max}$ of ∼100% orexin-A (Figure 3). Replacement of the pyridylmethyl with longer pyridylethyl groups resulted in decrease on potency at both receptors (**41** and **42**).

Finally, we examined whether the sulfonamide could be replaced with an amide (**43**−**44**, Table 5). Unfortunately, this structural modification resulted in significant reduction in potency at OX2R and total loss of activity at OX1R, similar to a previous report.[45] This clearly indicates the importance of the sulfonamide for activity at the orexin receptors.

**Computational Modeling Studies.** We built a full-length OX2R model based on the cryo-EM structures of agonist **5** (PDBID: 7L1V) and orexin-B-bound OX2R (PDBID: 7L1U) recently reported by Hong and colleagues[50] and a homology OX1R model based on the backbone and fold templates of the human OX2R structure, which shares 64% sequence identity with human OX1R.[2] The initial models were processed through a series of refinement steps employing MODELLER (simulated annealing with topological constraints),[61] AMBER18 low-mode exploration,[62−64] energy minimization, and dynamical equilibration in a lipid/KCl/water system employing the LIPID14 and ff14SB force fields.[65,66] We then explored agonists **5**, **2**, and **40** with OX2R and/or OX1R models via GLIDE-XP or SP docking,[67] distilling 120 minimized docked poses to the best 5, followed by induced


https://doi.org/10.1021/acs.jmedchem.1c00841
J. Med. Chem. 2021, 64, 8806−8825

**Table 2**

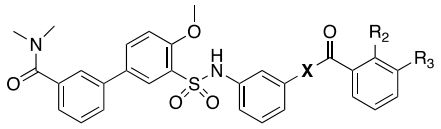

| No. | X | $R^2$ | $R^3$ | $OX_1R$ [a] $EC_{50}$ (nM) | $OX_1R$ [a] $E_{max}$ (%) | $OX_2R$ [a] $EC_{50}$ (nM) | $OX_2R$ [a] $E_{max}$ (%) | OX1R/OX2R |
|---|---|---|---|---|---|---|---|---|
| **17** | 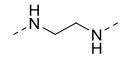 | H | $CH_3$ | 326 ± 51 | 112 ± 1 | 56 ± 26 | 98 ± 7 | 5.82 |
| **18** | 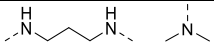 | H | | 931 ± 75 | 93 ± 3 | 406 ± 27 | 84 ± 2 | 2.29 |
| **19** | 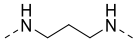 | H | $CH_3$ | 400 ± 47 | 103 ± 3 | 372 ± 19 | 78 ± 3 | 1.08 |
| **20** | 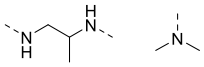 | H | | 2640 ± 530 | 76 ± 4[c] | 259 ± 6 | 92 ± 2 | 10.2 |
| **21** | 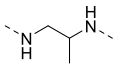 | H | $CH_3$ | 666 ± 100 | 94 ± 2 | 376 ± 38 | 82 ± 3 | 1.77 |
| **22** | 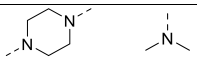 | H | | >10,000[b] | - | >10,000[b] | - | - |
| **23** | 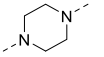 | H | $CH_3$ | >10,000[b] | - | >10,000[b] | - | - |

[a]$EC_{50}$ and $E_{max}$ values (% of orexin-A control) are the means ± SEM of at least three independent experiments conducted in duplicate. [b]Values are from two independent experiments conducted in duplicate. [c]Concentration−response curve does not have a top plateau.

fit modeling.[68] Molecular dynamics (MD) simulations were conducted with **40** in both OX2R and OX1R to identify key receptor−ligand interactions and probe their stability. Consistent with the cryo-EM OX2R structure, all compounds (**5**, **2**, and **40**) formed a "Z" shape in our OX2R model, kinked around the sulfonamide functionality with the two adjacent aromatic rings perpendicular to each other. The right end of these molecules inserted into the hydrophobic bottom of the pocket with the left end extending toward extracellular space (Figure 4A−C). This is consistent with the orexin-B bound cryo-EM structure showing the largely hydrophobic C-terminus residues of orexin-B, G24-I25-L26-T27-M28, bound at the hydrophobic bottom of the binding pocket.[50]

$Q134^{3.32}$ (Ballesteros−Weinstein numbering in superscript) was identified as the residue essential for binding and receptor activation in the agonist **5** and orexin-B-bound OX2R cryo-EM structures.[50] In both agonist-bound structures, the side chain of $Q134^{3.32}$ was extended and projected upward toward the extracellular side, as opposed to pointing more downward toward the cytoplasm in the antagonist-bound OX2R structures.[50,69,70] We observed the agonist-like orientation of the $Q134^{3.32}$ side chain in our OX2R model and such a conformation was largely maintained during 180 ns MD simulations of **40** in OX2R. $Q134^{3.32}$ was in close proximity of the sulfonamide group, as observed by Hong et al. in the **5**-bound OX2R cryo-EM structure[50] but was also close in space to the methoxy group on the neighboring aromatic ring in the initial induced fit docked poses in these agonists (Figure 4A,B). When MD simulations were performed on **40**, intimate and persistent hydrogen bond interactions of the $Q134^{3.32}$ amide group with the sulfonamide, sometimes bidentate as reported by Hong et al., were observed within 15 ns of the 180 ns MD simulation equilibration at 300 K, with additional hydrogen bond interactions, although slightly more distant, with the methoxy on the neighboring phenyl group (Figure 4C). These results clearly demonstrated the importance of the sulfonamide and are consistent with the SAR results where replacement of the sulfonamide with the corresponding amide (**43** and **44**) resulted in significant drop on potency at OX2R. In addition, it should be noted that all the active orexin agonists reported thus far (e.g., **2**−**5**, Figure 1) have a sulfonamide functionality.

In the OX1R homology model, **40** formed a similar "Z" shape, although slightly rotated (Figure 4D). Similar to the OX2R model, $Q126^{3.32}$ of OX1R, the equivalent residue of $Q134^{3.32}$ in OX2R, formed hydrogen bonding with the sulfonamide group and/or the neighboring methoxy group during the 180 ns MD simulations. In addition, hydrogen bonding between the sulfonamide group and $N318^{6.55}$ was also observed (Figure 4D). Markedly, as opposed to only transient interactions with $R339^{7.28}$ at the top of helix 7 in OX2R, the pyridylmethyl group on the left-hand side of **40** formed persistent hydrogen bonds or $\pi$-cation interactions with $R333^{7.29}$ in OX1R during the 180 ns MD simulations. Although additional studies are clearly needed, these receptor−ligand interactions, particularly via the pyridylmethyl group, may have contributed to the high potency of **40** in



https://doi.org/10.1021/acs.jmedchem.1c00841
J. Med. Chem. 2021, 64, 8806−8825

Table 3

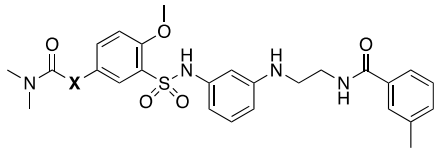

| No. | X | OX1R[a] | | OX2R[a] | | OX1R/ |
|---|---|---|---|---|---|---|
| | | $EC_{50}$ (nM) | $E_{max}$ (%) | $EC_{50}$ (nM) | $E_{max}$ (%) | OX2R |
| **24** | 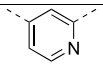 | 1810 ± 160 | 93 ± 3[c] | 683 ± 24 | 55 ± 5[c] | 2.65 |
| **25** | 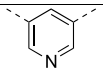 | 7530 ± 1040 | 105 ± 8[c] | 619 ± 57 | 78 ± 2[c] | 12.2 |
| **26** | 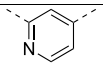 | 5170 ± 1060 | 101 ± 5[c] | 578 ± 90 | 85 ± 2[c] | 8.94 |
| **27** | 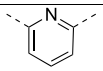 | 226 ± 40 | 100 ± 4 | 74 ± 12 | 94 ± 0 | 3.05 |
| **28** |  | 1330 ± 170 | 59 ± 5 | 166 ± 26 | 68 ± 4 | 8.00 |
| **29** |  | 2940 ± 460 | 35 ± 7[c] | 237 ± 60 | 72 ± 3 | 12.4 |
| **30** |  | 928 ± 120 | 51 ± 5 | 354 ± 69 | 43 ± 4 | 2.62 |
| **31** |  | >10,000[b] | - | >10,000[b] | - | - |
| **32** |  | >10,000[b] | - | >10,000[b] | - | - |

[a]$EC_{50}$ and $E_{max}$ values (% of orexin-A control) are the means ± SEM of at least three independent experiments conducted in duplicate. [b]Values are from two independent experiments conducted in duplicate. [c]Concentration−response curve does not have a top plateau.

OX1R, in contrast to OX2R agonists **2** and **5**, in which the pyridylmethyl motif is absent.

**Sleep Modulation Studies.** It has been previously shown that upon i.p. administration at 40 or 60 mg/kg, **2** increased wake time, as expected with OX2R agonists and decreased direct transitions from wakefulness to rapid eye movement (REM) sleep, a measure that is used to assess cataplexy, for 3 h[45,46] To test whether our OX agonists influence time spent awake and the transitions between sleep/wake states, we injected **40** into 12-month old female mice (40 mg/kg, i.p. during the quiet, lights-on phase) and measured sleep/wake parameters using continuous EEG/EMG recordings for 4 h postinjection. Compound **40** significantly increased active wakefulness and reduced nonrapid eye movement (NREM) and REM sleep relative to that after the vehicle injection (Figure 4A−C). There was a main effect of treatment on active wakefulness (Figure 4A, $P < 0.01$), NREM sleep (Figure 4B, $P < 0.05$), and REM sleep (Figure 4C, $P < 0.001$) during the 0−4 h postinjection time period.

To test whether **40** influences sleep patterns and quality, the total number of transitions between states, number, and the mean duration of episodes of each vigilance state were determined. Our data demonstrated that **40** stabilized behavior and reduced sleep/wake fragmentation, as indicated by reduced transitions between states (Figure 5D). In addition, **40**-induced enhancement of wake time was associated with an increase in average duration of wake episodes (Figure 5E). Whereas the agonist reduced number of wake episodes (Figure 5F), the increased duration of wake episodes resulted in overall enhancement of wake time following treatment. Similar to wake episodes, **40** increased the duration of NREM sleep episodes (Figure 5E). Reduced number of NREM sleep episodes (Figure 5F) following agonist administration resulted in overall reduction in time spent in NREM sleep. Surprisingly, **40** did not affect the duration of REM sleep episodes (Figure 5E), but fewer episodes of REM sleep (Figure 5F) resulted in overall reduction in REM sleep time following agonist administration. Together, these data demonstrate that **40** enhances wake, suppresses sleep, and reduces sleep/wake fragmentation. In particular, **40** enhances wake by increasing episode duration and decreases NREM and REM sleep by reducing the number, but not the duration, of episodes of NREM and REM sleep.

The wake-promoting effects observed with **40** were similar to those of orexin-A and the OX2R agonist **2** reported earlier. We have shown increased wakefulness and reduced NREM


https://doi.org/10.1021/acs.jmedchem.1c00841
J. Med. Chem. 2021, 64, 8806−8825

Table 4

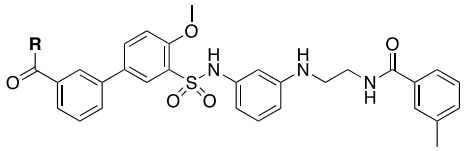

| No. | R | OX1R[a] | | OX2R[b] | | OX1R/ OX2R |
|---|---|---|---|---|---|---|
| | | $EC_{50}$ (nM) | $E_{max}$ (%) | $EC_{50}$ (nM) | $E_{max}$ (%) | |
| **33** | 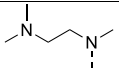 | 638 ± 120 | 102 ± 1 | 293 ± 3 | 85 ± 2 | 2.18 |
| **34** | 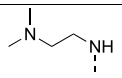 | >10,000[b] | - | 1630 ± 160 | 64 ± 4[c] | >6.13 |
| **35** |  | >10,000[b] | - | 450 ± 41 | 26 ± 0 | >22.2 |
| **36** | 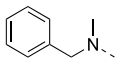 | >10,000[b] | - | 532 ± 220 | 61 ± 11 | >18.8 |
| **37** | 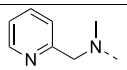 | 235 ± 45 | 96 ± 2 | 107 ± 4 | 76 ± 2 | 2.20 |
| **38** | 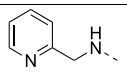 | >10,000[b] | - | 464 ± 55 | 22 ± 3 | >21.6 |
| **39** | 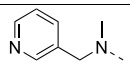 | 460 ± 44 | 98 ± 3 | 134 ± 24 | 75 ± 4 | 3.43 |
| **40** | 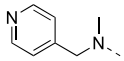 | 24 ± 6 | 104 ± 0 | 24 ± 4 | 96 ± 5 | 1.0 |
| **41** | 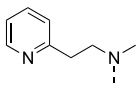 | 275 ± 25 | 112 ± 3 | 99 ± 20 | 90 ± 2 | 2.78 |
| **42** | 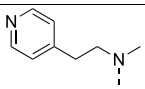 | 360 ± 58 | 116 ± 3 | 67 ± 20 | 97 ± 6 | 5.37 |

[a]$EC_{50}$ and $E_{max}$ values (% of orexin-A control) are the means ± SEM of at least three independent experiments conducted in duplicate. [b]Values are from two independent experiments conducted in duplicate. [c]Concentration−response curve does not have a top plateau.

and REM sleep following ventrolateral preoptic area injection of orexin-A in rats, which was associated with decreased NREM sleep and wake episodes 1 h postinjection.[25] i.c.v. administration of orexin-A (3 nmol) enhanced wakefulness and suppressed both NREM and REM sleep in mice up to 3 h following treatment.[53] Similarly, i.c.v. administered **2** (30, 100, and 300 nmol doses) during the light phase decreased percent time in NREM sleep and increased time in wakefulness up to 3 h postinjection. In addition, i.p. injected **2** (40 and 60 mg/kg, 6 h into the light phase) increased percent time in wakefulness and decreased percent time in REM sleep for up to 3 h following injections and the 40 mg/kg (i.p.) dose also reduced the percent time in NREM sleep in mice.[46] Notably, both the 40 and 60 mg/kg doses had identical wake-promoting effects, whereas the 20 mg/kg dose (i.p.) did not have any effect on the sleep/wake parameters. The relatively high doses required to affect sleep/wake cycles suggest that while **2** and **40** are able to reach the OX2R in the brain to modulate sleep, their brain penetration may be limited.

At 40 mg/kg, **40** and **2** produced similar wake-promoting effects upon i.p. administration, despite the significantly higher OX1R potency of **40**. This may reflect that OX2R plays a pivotal role in the modulation of sleep/wakefulness. It has been reported that OX2R KO mice exhibited a narcoleptic phenotype, whereas OX1R KO mice showed only a mild fragmentation of sleep and awake states.[71] In addition, while orexin-A effects on wake promotion and NREM sleep suppression were attenuated in both OX2R and OX1R KO mice, substantially greater reductions in OX2R KO mice (relative to OX1R KO mice) were observed.[53] Together, these


https://doi.org/10.1021/acs.jmedchem.1c00841
J. Med. Chem. 2021, 64, 8806−8825

Table 5

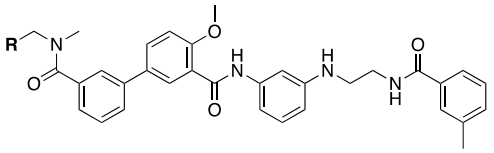

| No. | R | OX1R[a] | | OX2R[b] | | OX1R/ |
|---|---|---|---|---|---|---|
| | | $EC_{50}$ (nM) | $E_{max}$ (%) | $EC_{50}$ (nM) | $E_{max}$ (%) | OX2R |
| **43** | H | >10,000[b] | - | 1270 ± 260 | 11 ± 2 | >7.87 |
| **44** |  | >10,000[b] | - | 863 ± 300 | 10 ± 3 | >11.6 |

[a]$EC_{50}$ and $E_{max}$ values (% of orexin-A control) are the means ± SEM of at least three independent experiments conducted in duplicate. [b]Values are from two independent experiments conducted in duplicate.

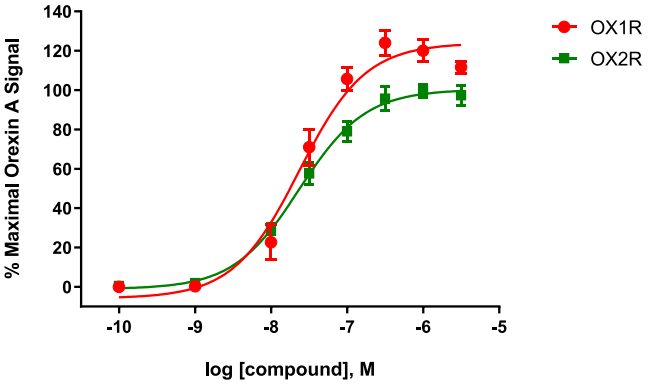


**Figure 3.** Activity of **40** in the OX1R and OX2R calcium mobilization assays. Each data point is the mean ± SEM of three independent experiments conducted in duplicate.

studies indicate that sleep appears to be primarily regulated by OX2R and to a lesser extent by OX1R; however, the role of the OX1R in sleep/wakefulness regulation may be best addressed when selective OX1R agonists become available.

## CONCLUSIONS

The orexin system is implicated in many physiological processes, and loss or decline has been associated with narcolepsy and other neurological diseases. Orexin agonists suitable for systemic administration have been suggested as the most promising strategy for the treatment of orexin deficiency-associated conditions among all orexin replacement therapies.[72,73] Compound **2** was one of the first small-molecule orexin agonists reported thus far, although it mainly activates OX2R with limited agonist activity at OX1R. Our SAR studies at multiple sites suggested that an amide functionality is required on ring-A at the left-hand side. Excitingly, introduction of a pyridylmethyl group at this amide increased potency at both OX1R and OX2R. Computational modeling studies based on the recently reported cryo-EM structure of OX2R bound with agonist **5** showed that **40** formed hydrogen bonding or $\pi$-cation interactions via the pyridylmethyl group with $R333^{7.29}$ in OX1R, which may have contributed to the observed high OX1R potency of **40**. Through this effort, we have identified dual OX agonists, including **40** (RTOXA-43),

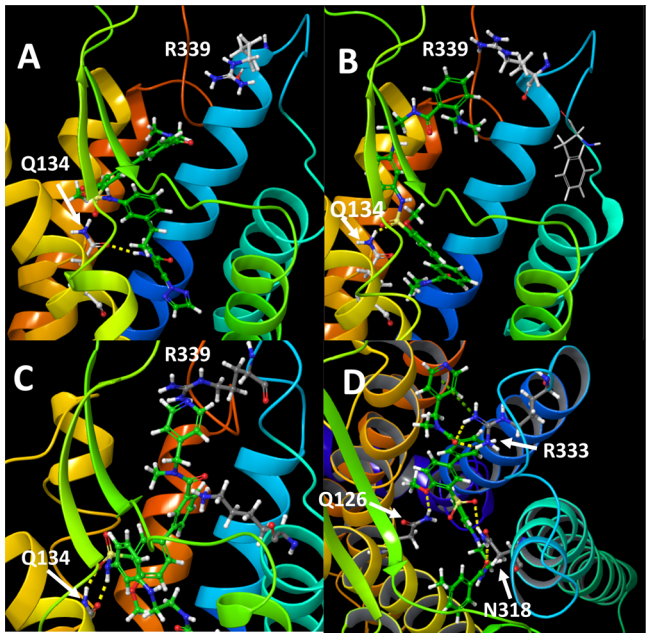


**Figure 4.** Induced fit top Emodel poses for (A) **5** in OX2R, (B) **2** in OX2R, (C) **40** in OX2R, and (D) **40** in OX1R full-length models based on the agonist-bound cryo-EM OX2R structures (7L1U and 7L1V). Ligands are in green and residues in gray.

which acted as a full agonist with $EC_{50}$ values of 24 nM at both OX receptors. These are the first and only small-molecule dual orexin agonists discovered thus far. When measured using continuous EEG/EMG recordings in 12-month-old mice, **40** (40 mg/kg, i.p.) increased time awake by increasing episode duration, decreased NREM and REM sleep, and improved sleep/wake consolidation by reducing the number, but not the duration, of episodes of NREM and REM sleep. The current results provide a promising lead for the discovery of small-molecule agonists with OX1R activities and support development of orexin agonists as potential treatments for orexin-deficient disorders such as narcolepsy.

## EXPERIMENTAL SECTION

**Chemistry.** All solvents and chemicals were reagent-grade. Unless otherwise mentioned, all reagents and solvents were purchased from


https://doi.org/10.1021/acs.jmedchem.1c00841
J. Med. Chem. 2021, 64, 8806−8825

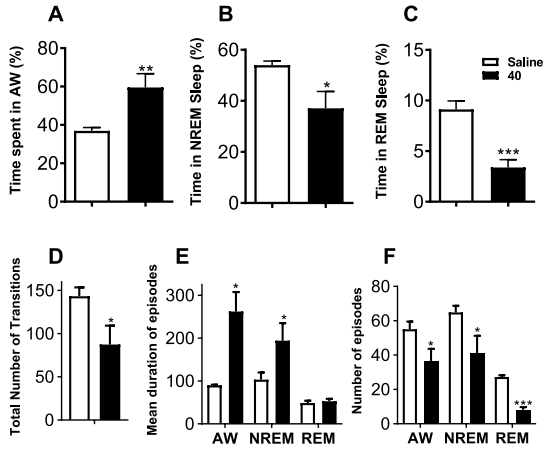


**Figure 5.** Intraperitoneal injection of **40** (40 mg/kg) during the quiet phase (lights-on) increased time spent in wakefulness (A), reduced time spent in NREM sleep (B), and REM sleep (C) 4 h postinjection. Agonist **40** also reduced the number of state transitions compared to saline injections (D), increased the duration of wake and NREM sleep episodes, without affecting the duration of REM sleep episodes (E), and reduced the number of episodes of wake, NREM, and REM sleep (F) 4 h postinjection. $n = 5$. Data represented as mean ± SEM. $^*P < 0.05$, $^{**}P < 0.01$ and $^{***}P < 0.001$. Note different scaling on $y$-axes.

commercial vendors and used as received. Flash column chromatography was carried out on a Teledyne ISCO CombiFlash Rf system using prepacked columns. Solvents used include hexane, ethyl acetate (EtOAc), dichloromethane, methanol, and chloroform/methanol/ammonium hydroxide (80:18:2) (CMA-80). Purity and characterization of compounds were established by a combination of high-performance liquid chromatography (HPLC), thin-layer chromatography (TLC), mass spectrometry, and NMR analyses. The melting point was recorded by the Mel-Temp II instrument (Laboratory Devices Inc., U.S.). $^1$H and $^{13}$C NMR spectra were recorded on a Bruker AVANCE DPX-300 (300 MHz) spectrometer and were determined in chloroform-$d$, DMSO-$d_6$, or methanol-$d_4$ with tetramethylsilane (0.00 ppm) or solvent peaks as the internal reference. Chemical shifts are reported in parts per million relative to the reference signal, and coupling constant ($J$) values are reported in hertz (Hz). TLC was performed on EMD precoated silica gel 60 F254 plates, and spots were visualized with UV light or iodine staining. Low-resolution mass spectra were obtained using a Waters Alliance HT/Micromass ZQ system (ESI). All test compounds were greater than 95% pure as determined by HPLC on an Agilent 1100 system using an Agilent Zorbax SB-Phenyl, 2.1 mm × 150 mm, 5 $\mu$m column using a 15 min gradient elution of 5−95% solvent B at 1 mL/min, followed by 10 min at 95% solvent B (solvent A, water with 0.1% TFA; solvent B, acetonitrile with 0.1% TFA and 5% water; absorbance monitored at 220 and 280 nm).

*tert-Butyl (2-((3-Nitrophenyl)amino)ethyl)carbamate (**45**).* 3-Nitrofluorobenzene (5.0 mmol, 35.4 mmol) and ethylenediamine (11.8 mL, 177.2 mmol) were mixed in a sealed tube, and the reaction was heated at 120 °C overnight. After cooling down, the volatile was evaporated under reduced pressure at 60 °C. The residue was then redissolved in a mixture of THF (30 mL) and water (30 mL), followed by the addition of potassium carbonate (14.7 g, 106.2 mmol) and di-*tert*-butyl ecarbonate (19.3 g, 88.5 mmol). The reaction was then stirred overnight and diluted by brine (150 mL). Ethyl acetate (150 mL) was then added, and the organic layer was separated and dried. The solvent was removed under reduced pressure, and the residue was purified by ISCO to afford the pure desired product. 6.28 g brown oil, yield: 63%. $^1$H NMR (300 MHz, chloroform-$d$): $\delta$ 7.51 (dd, $J$ = 1.60, 8.01 Hz, 1H), 7.37 (t, $J$ = 2.26 Hz, 1H), 7.22−7.31 (m, 1H), 6.87 (dd, $J$ = 2.07, 8.10 Hz, 1H), 4.78−4.94 (m, 1H), 4.56−4.73 (m, 1H), 3.36−3.50 (m, 2H), 3.21−3.34 (m, 2H), 1.38−1.50 (m, 9H). MS (ESI) $m/z$: 282.3 $[M + H]^+$; LCMS: >95% purity.

*tert-Butyl (2-(Benzyl(3-nitrophenyl)amino)ethyl)carbamate (**46**).* Compound **45** (6.28 g, 22.30 mmol) was dissolved in DMF (110 mL), followed by the addition of potassium carbonate (6.17 g, 44.65 mmol) and benzyl bromide (3.2 mL, 26.79 mmol). The reaction was then heated at 60 °C overnight. Water (500 mL) and ethyl acetate (200 mL) were added, and the organic layer was separated and dried. The solvent was removed under reduced pressure, and the residue was purified by ISCO to afford the pure desired product. 5.11 g orange syrup, yield: 62%. $^1$H NMR (300 MHz, chloroform-$d$): $\delta$ 7.46−7.59 (m, 2H), 7.34−7.40 (m, 1H), 7.26−7.34 (m, 3H), 7.17 (d, $J$ = 7.16 Hz, 2H), 7.02 (d, $J$ = 6.22 Hz, 1H), 4.58−4.76 (m, 3H), 3.57−3.72 (m, 2H), 3.37 (q, $J$ = 6.47 Hz, 2H), 1.35−1.48 (m, 9H). MS (ESI) $m/z$: 372.4 $[M + H]^+$.

*tert-Butyl (2-((3-Aminophenyl) (benzyl)amino)ethyl)carbamate (**47**).* Compound **46** (5.11 g, 13.76 mmol) was dissolved in a mixture of ethanol and water (55/22 mL), followed by the addition of ammonium chloride (7.36 g, 137.6 mmol) and iron powder (5.38 g, 96.3 mmol). The reaction was then heated at reflux for 3 h. After cooling down, DCM (100 mL) was added, and the mixture was filtered through Celite. The organic layer was then separated and dried. The solvent was then removed under reduced pressure and the residue was purified by ISCO to afford the desired product. 4.61 g brown oil, yield: 98%. $^1$H NMR (300 MHz, chloroform-$d$): $\delta$ 7.08−7.46 (m, 6H), 6.98 (t, $J$ = 8.19 Hz, 1H), 6.02−6.26 (m, 2H), 4.62−4.77 (m, 1H), 4.40−4.60 (m, 2H), 3.41−3.58 (m, 2H), 3.22−3.39 (m, 2H), 1.55−2.23 (m, 2H), 1.32−1.53 (m, 9H). MS (ESI) $m/z$: 342.2 $[M + H]^+$.

*tert-Butyl (2-(Benzyl(3-((5-bromo-2-methoxyphenyl)-sulfonamido)phenyl)amino)ethyl)carb-amate (**48**).* Under the protection of nitrogen, compound **47** (3.52 g, 10.31 mmol) was dissolved in anhydrous DCM (50 mL) at 0 °C. Pyridine (1 mL, 12.37 mmol) was added to the reaction, followed by the addition of 2-methoxy-5-bromobenzenesulfonyl chloride (3.24 g, 11.34 mmol). The reaction was warmed up to room temperature and stirred overnight. The reaction was quenched by saturated $NaHCO_3$ (30 mL), and DCM (100 mL) was added. The organic layer was separated and dried. The solvent was removed under reduced pressure and the residue was purified by ISCO to afford the desired product. 5.46 g off-white solid, yield: 90%. $^1$H NMR (300 MHz, chloroform-$d$): $\delta$ 7.87 (d, $J$ = 2.45 Hz, 1H), 7.55 (dd, $J$ = 2.45, 8.85 Hz, 1H), 7.18−7.35 (m, 4H), 7.10 (d, $J$ = 6.59 Hz, 2H), 7.00 (t, $J$ = 8.38 Hz, 1H), 6.90 (br s, 1H), 6.78 (d, $J$ = 8.85 Hz, 1H), 6.49 (d, $J$ = 8.48 Hz, 1H), 6.39 (d, $J$ = 4.71 Hz, 2H), 4.59−4.73 (m, 1H), 4.48 (s, 2H), 3.84 (s, 3H), 3.41−3.53 (m, 2H), 3.19−3.34 (m, 2H), 1.36−1.47 (m, 9H). MS (ESI) $m/z$: 592.2 $[M + H]^+$.

**General Procedure for the Synthesis of Compounds 2 and 6−16.** Compound **48** (1.0 equiv), boronic acid (1.2 equiv), $Pd(PPh_3)_4$ (0.1 equiv), and potassium carbonate (2.0 equiv) were placed in a round-bottomed flask with a condenser. The system was flushed with nitrogen, and a mixture of 1,4-dioxane/water (4/1, 0.1 M) was then added. The reaction was refluxed for 2 h. After cooling down, DCM (50 mL) was added and the organic layer was separated and dried. The solvent was removed to give crude compound **49** that was then dissolved in 4 N HCl in 1,4-dioxane (10 equiv). The reaction was stirred for 2 h at room temperature, and the solvent was then removed under reduced pressure. The residue was then dissolved in DMF (0.1 M), followed by the addition of 2-dimethylamino benzoic acid (1.1 equiv), HATU (1.2 equiv), and DIPEA (1.5 equiv). The reaction was stirred overnight at room temperature and quenched by saturated $NaHCO_3$. DCM (50 mL) was added, and the organic layer was separated and dried. The solvent was removed under reduced pressure to afford the crude product (compound **50**), which was then mixed with Pd/C (0.1 equiv) in MeOH (0.1 M) under the atmosphere of hydrogen (40 psi) for 12 h. The reaction mixture was filtered, and the solvent of the filtrate was removed under reduced pressure. The residue was purified by ISCO to afford the desired final products (**2**, **6−16**).

*3′-(N-(3-((2-(2-(Dimethylamino)benzamido)ethyl)amino)-phenyl)sulfamoyl)-4′-methoxy-N,N-dimethyl-[1,1′-biphenyl]-3-carboxamide (**2**).* Yield: 45% over four steps. $^1$H NMR (300 MHz,


https://doi.org/10.1021/acs.jmedchem.1c00841
J. Med. Chem. 2021, 64, 8806−8825

chloroform-*d*): δ 9.89 (br s, 1H), 8.00−8.17 (m, 2H), 7.64 (dd, *J* = 1.88, 8.67 Hz, 1H), 7.48−7.58 (m, 2H), 7.25−7.46 (m, 3H), 7.10−7.23 (m, 3H), 7.01 (d, *J* = 8.67 Hz, 1H), 6.94 (t, *J* = 8.01 Hz, 1H), 6.45 (br s, 1H), 6.34 (dd, *J* = 8.01, 14.79 Hz, 2H), 4.33 (br s, 1H), 3.94−4.09 (m, 3H), 3.54−3.73 (m, 2H), 3.28 (br s, 2H), 2.86−3.20 (m, 6H), 2.42−2.66 (m, 6H). MS (ESI) *m*/*z*: 616.3 $[M + H]^+$.

*3′-(N-(3-((2-(2-(Dimethylamino)benzamido)ethyl)amino)-phenyl)sulfamoyl)-N,N-diethyl-4′-methoxy-[1,1′-biphenyl]-3-carboxamide* (**6**). Yield: 29% over four steps. $^1$H NMR (300 MHz, chloroform-*d*): δ 9.90 (br s, 1H), 8.07−8.16 (m, 1H), 7.97−8.06 (m, 2H), 7.65 (dd, *J* = 2.26, 8.67 Hz, 1H), 7.46−7.54 (m, 2H), 7.41 (t, *J* = 7.54 Hz, 2H), 7.30 (d, *J* = 7.35 Hz, 1H), 7.12−7.22 (m, 2H), 7.03 (d, *J* = 8.67 Hz, 1H), 6.95 (t, *J* = 8.01 Hz, 1H), 6.44 (s, 1H), 6.34 (d, *J* = 5.09 Hz, 2H), 4.31 (t, *J* = 5.27 Hz, 1H), 4.07 (s, 3H), 3.65 (q, *J* = 5.84 Hz, 2H), 3.55 (br s, 2H), 3.17−3.36 (m, 4H), 2.75−2.99 (m, 6H), 1.26 (br s, 3H), 1.11 (br s, 3H). MS (ESI) *m*/*z*: 644.2 $[M + H]^+$.

*2-(Dimethylamino)-N-(2-((3-((4-methoxy-3′-(piperidine-1-carbonyl)-[1,1′-biphenyl])-3-sulfonamido)phenyl)amino)ethyl)-benzamide* (**7**). Yield: 36% over four steps. $^1$H NMR (300 MHz, chloroform-*d*): δ 9.67−9.90 (m, 1H), 8.03 (d, *J* = 2.07 Hz, 2H), 7.65−7.74 (m, 1H), 7.56−7.65 (m, 1H), 7.36−7.56 (m, 6H), 7.31 (s, 2H), 7.07 (s, 2H), 6.92 (br s, 2H), 6.79−6.87 (m, 1H), 4.04 (s, 3H), 3.79 (br s, 4H), 3.44 (br s, 4H), 3.14 (s, 6H), 1.69 (br s, 4H), 1.44−1.59 (m, 2H). MS (ESI) *m*/*z*: 656.3 $[M + H]^+$.

*2-(Dimethylamino)-N-(2-((3-((4-methoxy-3′-(pyrrolidine-1-carbonyl)-[1,1′-biphenyl])-3-sulfonamido)phenyl)amino)ethyl)-benzamide* (**8**). Yield: 39% over four steps. $^1$H NMR (300 MHz, chloroform-*d*): δ 9.90 (br s, 1H), 7.99−8.15 (m, 2H), 7.59−7.71 (m, 2H), 7.49−7.55 (m, 1H), 7.35−7.47 (m, 3H), 7.10−7.22 (m, 2H), 6.86−7.07 (m, 3H), 6.44 (s, 1H), 6.34 (dd, *J* = 4.71, 7.54 Hz, 2H), 4.23−4.39 (m, 1H), 4.06 (s, 3H), 3.56−3.72 (m, 8H), 3.42 (t, *J* = 6.50 Hz, 2H), 3.29 (t, *J* = 5.65 Hz, 2H), 2.82 (d, *J* = 8.10 Hz, 2H), 2.56 (s, 6H), 1.94−2.03 (m, 2H), 1.85−1.91 (m, 2H). MS (ESI) *m*/*z*: 642.2 $[M + H]^+$.

*3′-(N-(3-((2-(2-(Dimethylamino)benzamido)ethyl)amino)-phenyl)sulfamoyl)-4′-methoxy-N-p-ropyl-[1,1′-biphenyl]-3-carboxamide* (**9**). Yield: 32% over four steps. $^1$H NMR (300 MHz, chloroform-*d*): δ 9.87 (br s, 1H), 7.97−8.17 (m, 3H), 7.90 (s, 1H), 7.63−7.75 (m, 2H), 7.57 (d, *J* = 7.72 Hz, 1H), 7.33−7.49 (m, 2H), 7.10−7.23 (m, 2H), 7.02 (d, *J* = 4.33 Hz, 1H), 6.88−6.98 (m, 1H), 6.51 (br s, 1H), 6.44 (s, 1H), 6.32 (t, *J* = 6.59 Hz, 2H), 4.30 (br s, 1H), 4.05 (s, 3H), 3.60 (q, *J* = 5.78 Hz, 2H), 3.43 (q, *J* = 6.47 Hz, 2H), 3.26 (br s, 2H), 2.76−2.83 (m, 6H), 1.60−1.71 (m, 2H), 0.98 (t, *J* = 7.44 Hz, 3H). MS (ESI) *m*/*z*: 630.2 $[M + H]^+$.

*2-(Dimethylamino)-N-(2-((3-((3′-((dimethylamino)methyl)-4-methoxy-[1,1′-biphenyl])-3-sulfonamido)phenyl)amino)ethyl)-benzamide* (**10**). Yield: 26% over four steps. $^1$H NMR (300 MHz, chloroform-*d*): δ 9.89 (br s, 1H), 8.01−8.16 (m, 2H), 7.67 (dd, *J* = 2.35, 8.57 Hz, 1H), 7.22−7.51 (m, 6H), 7.06−7.22 (m, 3H), 6.81−7.04 (m, 2H), 6.46 (d, *J* = 1.88 Hz, 1H), 6.25−6.42 (m, 2H), 4.14−4.41 (m, 1H), 3.98−4.11 (m, 3H), 3.63 (q, *J* = 5.78 Hz, 2H), 3.47 (s, 2H), 3.28 (t, *J* = 5.65 Hz, 2H), 2.47−2.62 (m, 6H), 2.26 (s, 6H). MS (ESI) *m*/*z*: 602.4 $[M + H]^+$.

*2-(Dimethylamino)-N-(2-((3-((3′-(dimethylamino)-4-methoxy-[1,1′-biphenyl])-3-sulfonamido)phenyl)amino)ethyl)benzamide* (**11**). Yield: 35% over four steps. $^1$H NMR (300 MHz, $CDCl_3$): δ 9.92 (br s, 1H), 8.11 (d, *J* = 7.72 Hz, 1H), 8.05 (d, *J* = 2.26 Hz, 1H), 7.66 (dd, *J* = 2.26, 8.48 Hz, 1H), 7.31−7.51 (m, 1H), 7.06−7.24 (m, 3H), 6.84−7.05 (m, 3H), 6.73−6.84 (m, 2H), 6.70 (d, *J* = 10.17 Hz, 1H), 6.45 (s, 1H), 6.31 (d, *J* = 7.91 Hz, 2H), 3.97−4.09 (m, 3H), 3.53−3.69 (m, 2H), 3.29 (t, *J* = 5.75 Hz, 2H), 2.29−3.06 (m, 12H). MS (ESI) *m*/*z*: 588.2 $[M + H]^+$.

*2-(Dimethylamino)-N-(2-((3-((3′-isopropyl-4-methoxy-[1,1′-biphenyl])-3-sulfonamido)phenyl)amino)ethyl)benzamide* (**12**). Yield: 41% over four steps. $^1$H NMR (300 MHz, chloroform-*d*): δ 9.91 (br s, 1H), 8.11 (dd, *J* = 1.70, 7.91 Hz, 1H), 8.05 (d, *J* = 2.26 Hz, 1H), 7.65 (dd, *J* = 2.35, 8.57 Hz, 1H), 7.37−7.45 (m, 1H), 7.28−7.36 (m, 3H), 7.20 (d, *J* = 7.35 Hz, 2H), 7.08−7.16 (m, 1H), 7.02 (d, *J* = 8.67 Hz, 1H), 6.94 (t, *J* = 8.10 Hz, 1H), 6.89 (s, 1H), 6.45 (t, *J* = 2.07 Hz, 1H), 6.33 (td, *J* = 2.28, 8.05 Hz, 2H), 4.17−4.54 (m, 1H), 4.05−4.09 (m, 3H), 3.64 (q, *J* = 5.97 Hz, 2H), 3.29 (t, *J* = 5.75 Hz, 2H), 2.87−2.99 (m, 1H), 2.54 (s, 6H), 1.27 (d, *J* = 6.97 Hz, 6H). MS (ESI) *m*/*z*: 587.2 $[M + H]^+$.

*N-(2-((3-((3′-(Diethylamino)-4-methoxy-[1,1′-biphenyl])-3-sulfonamido)phenyl)amino)ethyl-)-2-(dimethylamino)benzamide* (**13**). Yield: 32% over four steps. $^1$H NMR (300 MHz, chloroform-*d*): δ 9.93 (br s, 1H), 8.11 (dd, *J* = 1.70, 7.91 Hz, 1H), 8.04 (d, *J* = 2.26 Hz, 1H), 7.64 (dd, *J* = 2.26, 8.67 Hz, 1H), 7.36−7.46 (m, 1H), 7.07−7.24 (m, 3H), 7.00 (d, *J* = 8.67 Hz, 1H), 6.87−6.96 (m, 2H), 6.69−6.77 (m, 2H), 6.65 (d, *J* = 8.10 Hz, 1H), 6.45 (d, *J* = 2.07 Hz, 1H), 6.27−6.38 (m, 2H), 4.05 (s, 3H), 3.64 (q, *J* = 5.97 Hz, 2H), 3.38 (q, *J* = 7.16 Hz, 3H), 3.29 (t, *J* = 5.75 Hz, 2H), 2.43−2.60 (m, 6H), 1.17 (t, *J* = 7.06 Hz, 6H). MS (ESI) *m*/*z*: 616.2 $[M + H]^+$.

*2-(Dimethylamino)-N-(2-((3-((3′-(dipropylamino)-4-methoxy-[1,1′-biphenyl])-3-sulfonamido)phenyl)amino)ethyl)benzamide* (**14**). Yield: 33% over four steps. $^1$H NMR (300 MHz, chloroform-*d*): δ 9.93 (br s, 1H), 8.11 (dd, *J* = 1.70, 7.72 Hz, 1H), 8.03 (d, *J* = 2.45 Hz, 1H), 7.63 (dd, *J* = 2.35, 8.57 Hz, 1H), 7.40 (dt, *J* = 1.70, 7.72 Hz, 1H), 7.10−7.24 (m, 3H), 7.01 (d, *J* = 8.67 Hz, 1H), 6.93 (t, *J* = 8.01 Hz, 1H), 6.88 (s, 1H), 6.65−6.73 (m, 2H), 6.61 (dd, *J* = 2.26, 8.29 Hz, 1H), 6.44 (t, *J* = 2.07 Hz, 1H), 6.27−6.36 (m, 2H), 4.05 (s, 3H), 3.64 (q, *J* = 5.84 Hz, 1H), 3.16−3.33 (m, 4H), 2.49−2.58 (m, 6H), 1.57−1.64 (m, 4H), 0.93 (t, *J* = 7.44 Hz, 6H). MS (ESI) *m*/*z*: 644.2 $[M + H]^+$.

*N-(2-((3-((3′-(tert-Butyl)-4-methoxy-[1,1′-biphenyl])-3-sulfonamido)phenyl)amino)ethyl)-2-(dimethylamino)benzamide* (**15**). Yield: 39% over four steps. $^1$H NMR (300 MHz, chloroform-*d*): δ 9.77−10.00 (m, 1H), 8.11 (dd, *J* = 1.60, 7.82 Hz, 1H), 8.04 (d, *J* = 2.26 Hz, 1H), 7.65 (dd, *J* = 2.35, 8.57 Hz, 1H), 7.47 (s, 1H), 7.39 (dd, *J* = 1.70, 7.54 Hz, 1H), 7.32−7.37 (m, 1H), 7.28−7.31 (m, 1H), 7.26 (s, 1H), 7.15−7.22 (m, 1H), 7.12 (d, *J* = 8.10 Hz, 1H), 7.03 (d, *J* = 8.67 Hz, 1H), 6.88−6.99 (m, 2H), 6.43−6.49 (m, 1H), 6.27−6.38 (m, 2H), 4.06 (s, 3H), 3.57−3.70 (m, 2H), 3.29 (t, *J* = 5.84 Hz, 2H), 2.42−2.60 (m, 6H), 1.29−1.38 (m, 9H). MS (ESI) *m*/*z*: 601.2 $[M + H]^+$.

*2-(Dimethylamino)-N-(2-((3-((4-methoxy-3′-(trifluoromethyl)-[1,1′-biphenyl])-3-sulfonamido)phenyl)amino)ethyl)benzamide* (**16**). Yield: 31% over four steps. $^1$H NMR (300 MHz, chloroform-*d*): δ 9.91 (br s, 1H), 8.11 (dd, *J* = 1.70, 7.91 Hz, 1H), 8.04 (d, *J* = 2.45 Hz, 1H), 7.70 (s, 1H), 7.61−7.68 (m, 2H), 7.55−7.60 (m, 1H), 7.52 (d, *J* = 7.54 Hz, 1H), 7.42 (dt, *J* = 1.79, 7.68 Hz, 1H), 7.20 (d, *J* = 7.72 Hz, 1H), 7.14 (d, *J* = 8.10 Hz, 1H), 7.06 (d, *J* = 8.67 Hz, 1H), 6.89−6.99 (m, 2H), 6.39−6.49 (m, 1H), 6.34 (d, *J* = 8.10 Hz, 2H), 4.21−4.57 (m, 1H), 4.06−4.13 (m, 3H), 3.65 (q, *J* = 5.97 Hz, 2H), 3.29 (t, *J* = 5.75 Hz, 2H), 2.48−2.62 (m, 6H). MS (ESI) *m*/*z*: 613.2 $[M + H]^+$.

**General Procedure for the Synthesis of Compound 51a−b.** 3-Nitrofluorobenzene (1 equiv) and the appropriate diamine (5 equiv) were mixed in a sealed tube, and the reaction was heated at 120 °C overnight. After cooling down, the volatile was evaporated under reduced pressure at 60 °C. The residue was then redissolved in a mixture of THF (30 mL) and water (30 mL), followed by the addition of potassium carbonate (3.0 equiv) and di-*tert*-butyl dicarbonate (2.5 equiv). The reactant was then stirred overnight and diluted by brine (150 mL). Ethyl acetate (150 mL) was then added, and the organic layer was separated and dried. The solvent was removed under reduced pressure, and the residue was purified by ISCO to afford the pure desired product.

*tert-Butyl (3-((3-Nitrophenyl)amino)propyl)carbamate* (**51a**). Yield: 72%. $^1$H NMR (300 MHz, chloroform-*d*): δ 7.50 (dd, *J* = 1.60, 8.01 Hz, 1H), 7.39 (t, *J* = 2.26 Hz, 1H), 7.25−7.30 (m, 1H), 6.88 (dd, *J* = 2.07, 8.10 Hz, 1H), 4.56−4.69 (m, 1H), 3.25 (dq, *J* = 3.58, 6.34 Hz, 4H), 2.72 (d, *J* = 7.16 Hz, 1H), 1.79 (t, *J* = 6.50 Hz, 2H), 1.45 (s, 9H). MS (ESI) *m*/*z*: 296.2 $[M + H]^+$.

*tert-Butyl (1-((3-Nitrophenyl)amino)propan-2-yl)carbamate* (**51b**). Yield: 30%. $^1$H NMR (300 MHz, chloroform-*d*): δ 7.47−7.52 (m, 2H), 7.35 (t, *J* = 2.26 Hz, 2H), 7.24−7.29 (m, 1H), 6.87 (dd, *J* = 1.88, 8.10 Hz, 1H), 4.78−4.87 (m, 1H), 4.46−4.59 (m, 1H), 3.92−4.03 (m, 1H), 3.21 (s, 2H), 3.06−3.15 (m, 1H), 2.74−2.92 (m, 1H), 1.40−1.47 (m, 9H), 1.24−1.28 (m, 3H). MS (ESI) *m*/*z*: 296.2 $[M + H]^+$.


https://doi.org/10.1021/acs.jmedchem.1c00841
J. Med. Chem. 2021, 64, 8806−8825

**General Procedure for the Synthesis of Compound 52a−b.** Compound **51a** or **51b** (1 equiv) was dissolved in DMF (0.2 M), followed by the addition of potassium carbonate (2 equiv) and benzyl bromide (1.2 equiv). The reaction was then heated at 60 °C overnight. Water and ethyl acetate were added, and the organic layer was separated and dried. The solvent was removed under reduced pressure, and the residue was purified by ISCO to afford the desired product **52a−b**.

*tert-Butyl (3-(Benzyl(3-nitrophenyl)amino)propyl)carbamate (**52a**).* Yield: 84%. $^1$H NMR (300 MHz, chloroform-*d*): $\delta$ 7.46−7.54 (m, 2H), 7.28−7.39 (m, 3H), 7.25−7.27 (m, 1H), 7.18 (d, $J$ = 6.78 Hz, 2H), 6.86−6.96 (m, 1H), 4.60 (s, 2H), 3.45−3.58 (m, 1H), 3.21 (d, $J$ = 6.40 Hz, 1H), 1.82−1.94 (m, 2H), 1.44 (s, 9H). MS (ESI) $m/z$: 386.2 $[M + H]^+$.

*tert-Butyl (1-(Benzyl(3-nitrophenyl)amino)propan-2-yl)carbamate (**52b**).* Yield: 81%. $^1$H NMR (300 MHz, chloroform-*d*): $\delta$ 7.58 (br s, 1H), 7.48 (dd, $J$ = 1.51, 7.91 Hz, 1H), 7.37 (d, $J$ = 4.33 Hz, 1H), 7.25−7.32 (m, 4H), 7.17 (s, 1H), 6.97−7.12 (m, 1H), 4.59−4.77 (m, 3H), 4.27−4.50 (m, 1H), 4.09 (d, $J$ = 6.97 Hz, 1H), 3.21−3.82 (m, 2H), 1.31−1.46 (m, 9H). MS (ESI) $m/z$: 386.1 $[M + H]^+$.

**General Procedure for the Synthesis of Compound 53a−b.** Compound **52a** or **52b** (1 equiv) was dissolved in the mixture of ethanol and water (5:2, 0.2 M), followed by the addition of ammonium chloride (10 equiv) and iron powder (7 equiv). The reaction was then heated at reflux for 3 h. After cooling down, DCM (100 mL) was added and the mixture was filtered through Celite. The organic layer was then separated and dried. The solvent was then removed under reduced pressure, and the residue was purified by ISCO to afford the desired product **53a−b**.

*tert-Butyl N-{3-[(3-Aminophenyl)(benzyl)amino]propyl}carbamate (**53a**).* Yield: 92%. $^1$H NMR (300 MHz, chloroform-*d*): $\delta$ 7.27−7.40 (m, 2H), 7.18−7.25 (m, 3H), 6.97 (t, $J$ = 8.01 Hz, 1H), 5.98−6.21 (m, 3H), 4.49 (m, 3H), 3.29−3.45 (m, 2H), 3.15 (d, $J$ = 6.22 Hz, 2H), 1.74−1.88 (m, 2H), 1.43 (s, 9H). MS (ESI) $m/z$: 356.2 $[M + H]^+$.

*tert-Butyl N-{1-[(3-Aminophenyl)(benzyl)amino]propan-2-yl}carbamate (**53b**).* Yield: 92%. $^1$H NMR (300 MHz, chloroform-*d*): $\delta$ 7.37 (d, $J$ = 4.33 Hz, 1H), 7.26−7.32 (m, 2H), 7.18 (t, $J$ = 6.69 Hz, 2H), 6.96 (t, $J$ = 8.10 Hz, 1H), 6.23 (dd, $J$ = 2.45, 8.29 Hz, 1H), 6.12−6.19 (m, 1H), 6.06 (dd, $J$ = 1.51, 7.72 Hz, 1H), 4.49−4.73 (m, 2H), 4.35−4.48 (m, 1H), 3.95−4.09 (m, 1H), 3.45−3.69 (m, 2H), 3.08−3.22 (m, 1H), 1.29−1.48 (m, 9H), 1.18 (d, $J$ = 6.78 Hz, 3H). MS (ESI) $m/z$: 356.2 $[M + H]^+$.

**General Procedure for the Synthesis of Compound 54a−b.** Under the protection of nitrogen, compound **53a** or **53b** (1 equiv) was dissolved in anhydrous DCM (0.2 equiv) at 0 °C, pyridine (1.2 equiv) was added, followed by the addition of 2-methoxy-5-bromobenzenesulfonyl chloride (1.1 equiv). The reaction was warmed up to room temperature and stirred overnight. The reaction was quenched with saturated $NaHCO_3$ (10 mL), and DCM (30 mL) was added. The organic layer was separated and dried. The solvent was removed under reduced pressure, and the residue was purified by ISCO to afford the desired products **54a−b**.

*tert-Butyl (3-(Benzyl(3-((5-bromo-2-methoxyphenyl)sulfonamido)phenyl)amino)propyl)carbamate (**54a**).* Yield: 85%. $^1$H NMR (300 MHz, chloroform-*d*): $\delta$ 7.88 (d, $J$ = 2.64 Hz, 1H), 7.55 (dd, $J$ = 2.64, 8.85 Hz, 1H), 7.28 (d, $J$ = 7.54 Hz, 2H), 7.23 (s, 1H), 7.11 (d, $J$ = 6.59 Hz, 2H), 6.97 (d, $J$ = 8.10 Hz, 1H), 6.92 (s, 1H), 6.79 (d, $J$ = 8.85 Hz, 1H), 6.37−6.46 (m, 2H), 6.33 (d, $J$ = 8.67 Hz, 1H), 4.54−4.64 (m, 1H), 4.44 (s, 2H), 3.85 (s, 3H), 3.30−3.42 (m, 2H), 3.15 (d, $J$ = 6.22 Hz, 2H), 1.70−1.83 (m, 2H), 1.44 (s, 9H). MS (ESI) $m/z$: 606.2 $[M + H]^+$.

*tert-Butyl (1-(Benzyl(3-((5-bromo-2-methoxyphenyl)sulfonamido)phenyl)amino)propan-2-yl)carbamate (**54b**).* Yield: 83%. $^1$H NMR (300 MHz, chloroform-*d*): $\delta$ 7.86 (d, $J$ = 2.64 Hz, 1H), 7.54 (dd, $J$ = 2.45, 8.85 Hz, 1H), 7.25−7.30 (m, 3H), 7.07 (d, $J$ = 6.59 Hz, 2H), 6.99 (t, $J$ = 8.10 Hz, 1H), 6.90 (br s, 1H), 6.70−6.83 (m, 1H), 6.52 (d, $J$ = 8.48 Hz, 1H), 6.34−6.46 (m, 2H), 4.42−4.64 (m, 2H), 4.33 (d, $J$ = 12.06 Hz, 1H), 3.90−4.05 (m, 1H), 3.79−3.88 (m, 3H), 3.58 (br s, 1H), 3.18 (br s, 1H), 1.37 (s, 9H), 1.16 (d, $J$ = 6.59 Hz, 2H). MS (ESI) $m/z$: 606.2 $[M + H]^+$.

**General Procedure for the Synthesis of Compounds 17−21.** Compound **48**, **54a**, or **54b** (1.0 equiv), boronic acid (1.2 equiv), $Pd(PPh_3)_4$ (0.1 equiv), and potassium carbonate (2.0 equiv) were placed in a round-bottomed flask with an efficient condenser. The system was then flushed with nitrogen, and a mixture of 1,4-dioxane/water (4/1, 0.1 M) was added. The reaction was refluxed for 2 h. After cooling down, DCM (50 mL) was added and the organic layer was separated and dried. The solvent was then removed, and the residue (intermediate compound **53**) was dissolved in 4 N HCl in 1,4-dioxane (10 equiv). The reaction was stirred for 2 h at room temperature, and the solvent was then removed under reduced pressure to give a brown solid that was then dissolved in DMF (0.1 M), followed by the addition of the corresponding benzoic acid (1.1 equiv), HATU (1.2 equiv), and DIPEA (1.5 equiv). The reaction was stirred overnight at room temperature and quenched by saturated $NaHCO_3$. DCM (50 mL) was added and the organic layer was separated and dried. The solvent was removed under reduced pressure to afford the crude product (compound **54a−c**), which was then mixed with Pd/C (0.1 equiv) in MeOH (0.1 M) under the atmosphere of hydrogen (40 psi) for 12 h. The reaction mixture was filtered, and the solvent of the filtrate was removed under reduced pressure. The residue was purified by ISCO to afford the desired final products **17−21**.

*4′-Methoxy-N,N-dimethyl-3′-(N-(3-((2-(3-methylbenzamido)ethyl)amino)phenyl)sulfamoyl-)-[1,1′-biphenyl]-3-carboxamide (**17**).* $^1$H NMR (300 MHz, chloroform-*d*): $\delta$ 9.89 (br s, 1H), 8.00−8.17 (m, 2H), 7.64 (dd, $J$ = 1.88, 8.67 Hz, 1H), 7.48−7.58 (m, 2H), 7.25−7.46 (m, 3H), 7.10−7.23 (m, 3H), 7.01 (d, $J$ = 8.67 Hz, 1H), 6.94 (t, $J$ = 8.01 Hz, 1H), 6.45 (br s, 1H), 6.34 (dd, $J$ = 8.01, 14.79 Hz, 2H), 4.33 (br s, 1H), 3.94−4.09 (m, 3H), 3.54−3.73 (m, 2H), 3.28 (br s, 2H), 2.86−3.20 (m, 6H), 2.42−2.66 (m, 6H). MS (ESI) $m/z$: 587.2 $[M + H]^+$.

*3′-(N-(3-((3-(2-(Dimethylamino)benzamido)propyl)amino)-phenyl)sulfamoyl)-4′-methoxy-N,N-dimethyl-[1,1′-biphenyl]-3-carboxamide (**18**).* Yield: 29% over four steps. $^1$H NMR (300 MHz, chloroform-*d*): $\delta$ 9.71 (br s, 1H), 7.97−8.15 (m, 2H), 7.62−7.80 (m, 2H), 7.50−7.57 (m, 2H), 7.30−7.48 (m, 4H), 7.14−7.22 (m, 2H), 7.02−7.10 (m, 1H), 6.88−6.97 (m, 2H), 6.39−6.53 (m, 1H), 6.20−6.37 (m, 2H), 4.03−4.10 (m, 3H), 3.31−3.54 (m, 2H), 2.78−3.21 (m, 12H), 2.38−2.64 (m, 2H), 1.74−1.90 (m, 2H). MS (ESI) $m/z$: 630.2 $[M + H]^+$.

*4′-Methoxy-N,N-dimethyl-3′-(N-(3-((3-(3-methylbenzamido)propyl)amino)phenyl)sulfamoyl)-[1,1′-biphenyl]-3-carboxamide (**19**).* Yield: 32% over four steps. $^1$H NMR (300 MHz, chloroform-*d*): $\delta$ 8.08 (d, $J$ = 2.45 Hz, 1H), 7.71−8.04 (m, 1H), 7.67 (dd, $J$ = 2.35, 8.57 Hz, 1H), 7.57 (s, 1H), 7.52 (td, $J$ = 1.53, 3.53 Hz, 3H), 7.29−7.45 (m, 3H), 7.04 (d, $J$ = 8.85 Hz, 2H), 6.85−6.98 (m, 2H), 6.48 (d, $J$ = 1.88 Hz, 1H), 6.25−6.35 (m, 2H), 4.13 (s, 1H), 4.02−4.08 (m, 4H), 3.36 (q, $J$ = 6.22 Hz, 2H), 2.76−3.23 (m, 14H), 2.35 (s, 3H), 1.69−1.74 (m, 3H). MS (ESI) $m/z$: 601.2 $[M + H]^+$.

*3′-(N-(3-((2-(2-(Dimethylamino)benzamido)propyl)amino)-phenyl)sulfamoyl)-4′-methoxy-N,N-dimethyl-[1,1′-biphenyl]-3-carboxamide (**20**).* Yield: 22% over four steps. $^1$H NMR (300 MHz, chloroform-*d*): $\delta$ 9.70−9.79 (m, 1H), 8.01−8.11 (m, 2H), 7.64 (dd, $J$ = 2.45, 8.67 Hz, 1H), 7.49−7.56 (m, 2H), 7.38−7.47 (m, 2H), 7.30−7.37 (m, 1H), 7.11−7.23 (m, 2H), 6.97−7.06 (m, 2H), 6.93 (t, $J$ = 8.01 Hz, 1H), 6.42 (t, $J$ = 1.98 Hz, 1H), 6.25−6.38 (m, 2H), 4.35−4.46 (m, 1H), 4.06 (s, 3H), 3.13−3.20 (m, 2H), 2.85−3.06 (m, 7H), 2.80 (s, 6H), 1.28 (d, $J$ = 6.78 Hz, 3H). MS (ESI) $m/z$: 630.2 $[M + H]^+$.

*4′-Methoxy-N,N-dimethyl-3′-(N-(3-((2-(3-methylbenzamido)propyl)amino)phenyl)sulfamoyl)-[1,1′-biphenyl]-3-carboxamide (**21**).* Yield: 19% over four steps. $^1$H NMR (300 MHz, chloroform-*d*): $\delta$ 8.09 (d, $J$ = 2.45 Hz, 1H), 8.01 (s, 1H), 7.65 (dd, $J$ = 2.45, 8.67 Hz, 1H), 7.48−7.59 (m, 4H), 7.41 (t, $J$ = 7.72 Hz, 1H), 7.30−7.35 (m, 1H), 7.24 (s, 1H), 7.11 (s, 1H), 7.01 (d, $J$ = 8.67 Hz, 1H), 6.90 (t, $J$ = 8.01 Hz, 1H), 6.72 (d, $J$ = 8.10 Hz, 1H), 6.46 (t, $J$ = 1.98 Hz, 1H), 6.29 (dt, $J$ = 1.79, 7.86 Hz, 2H), 4.39−4.47 (m, 1H), 4.02 (s, 3H),


https://doi.org/10.1021/acs.jmedchem.1c00841
J. Med. Chem. 2021, 64, 8806−8825

3.00 (s, 2H), 2.80 (s, 6H), 2.32 (s, 3H), 1.25 (d, $J$ = 6.78 Hz, 3H). MS (ESI) $m/z$: 601.2 $[M + H]^+$.

*tert-Butyl 4-(3-Nitrophenyl)piperazine-1-carboxylate (**57**).* 3-Nitrofluorobenzene (5.0 mmol, 35.4 mmol) and piperazine (9.16 g, 106.31 mmol) were mixed in a sealed tube, and the reaction was heated at 120 °C overnight. After cooling down, the volatile was evaporated under reduced pressure at 60 °C. The residue was then redissolved in the mixture of THF (30 mL) and water (30 mL), followed by the addition of potassium carbonate (14.7 g, 106.2 mmol) and di-*tert*-butyl dicarbonate (19.3 g, 88.5 mmol). The reaction was then stirred overnight and diluted by brine (150 mL). Ethyl acetate (150 mL) was then added, and the organic layer was separated and dried. The solvent was removed under reduced pressure, and the residue was purified by ISCO to afford the desired product. 5.30 g as a yellow solid, yield: 49%. $^1$H NMR (300 MHz, chloroform-*d*): $\delta$ 7.64−7.76 (m, 2H), 7.40 (t, $J$ = 8.10 Hz, 1H), 7.16−7.24 (m, 1H), 3.54−3.67 (m, 2H), 3.19−3.30 (m, 4H), 1.49 (s, 9H). MS (ESI) $m/z$: 308.2 $[M + H]^+$.

*tert-Butyl 4-(3-Aminophenyl)piperazine-1-carboxylate (**58**).* Compound **57** (5.35 g, 17.41 mmol) was dissolved in the mixture of ethanol and water (70/30 mL), followed by the addition of ammonium chloride (9.31 g, 174.1 mmol) and iron powder (6.81 g, 121.8 mmol). The reaction was then heated at reflux for 3 h. After cooling down, DCM (100 mL) was added, and the mixture was filtered through Celite. The organic layer was then separated and dried. The solvent was then removed under reduced pressure, and the residue was purified by ISCO to afford the pure desired product. 4.15 g brown oil, yield: 86%. $^1$H NMR (300 MHz, chloroform-*d*): $\delta$ 6.98−7.11 (m, 1H), 6.32−6.39 (m, 1H), 6.20−6.30 (m, 2H), 3.58−3.85 (m, 2H), 3.49−3.58 (m, 4H), 3.07−3.14 (m, 4H), 1.47−1.50 (m, 9H). MS (ESI) $m/z$: 278.2 $[M + H]^+$.

*tert-Butyl 4-(3-((5-Bromo-2-methoxyphenyl)sulfonamido)-phenyl)piperazine-1-carboxylate (**59**).* Under the protection of nitrogen, compound **58** (3.04 g, 10.96 mmol) was dissolved in anhydrous DCM (55 mL) at 0 °C, pyridine (1.06 mL, 13.15 mmol) was added, followed by the addition of 2-methoxy-5-bromobenzene-sulfonyl chloride (3.44 g, 12.06 mmol). The reaction was warmed up to room temperature and stirred overnight. The reaction was quenched by saturated $NaHCO_3$ (30 mL), and DCM (100 mL) was added. The organic layer was separated and dried. The solvent was removed under reduced pressure, and the residue was purified by ISCO to afford the desired product **57**. 4.61 g brown solid, yield: 80%. $^1$H NMR (300 MHz, chloroform-*d*): $\delta$ 7.94 (d, $J$ = 2.45 Hz, 1H), 7.58 (dd, $J$ = 2.54, 8.76 Hz, 1H), 7.26 (s, 3H), 7.07 (t, $J$ = 8.10 Hz, 1H), 6.82−6.93 (m, 2H), 6.69−6.76 (m, 1H), 6.64 (d, $J$ = 8.29 Hz, 1H), 6.41 (d, $J$ = 7.91 Hz, 1H), 4.01 (s, 3H), 3.48−3.62 (m, 4H), 3.00−3.16 (m, 4H), 1.48 (s, 9H). MS (ESI) $m/z$: 528.2 $[M + H]^+$.

**General Procedure for the Synthesis of 22 and 23.** Compound **59** (1.0 equiv), boronic acid (1.2 equiv), $Pd(PPh_3)_4$ (0.1 equiv), and potassium carbonate (2.0 equiv) were placed in a round-bottomed flask with an efficient condenser. The system was then flushed with nitrogen, and a mixture of 1,4-dioxane/water (4/1, 0.1 M) was added. The reaction was refluxed for 2 h. After cooling down, DCM (50 ml) was added and the organic layer was separated and dried. The solvent was then removed, and the residue (compound **58**) was dissolved in 4 N HCl in 1,4-dioxane (10 equiv). The reaction was stirred for 2 h at room temperature, and the solvent was then removed under reduced pressure. The residue was then dissolved in DMF (0.1 M), followed by the addition of the corresponding benzoic acid (1.1 equiv), HATU (1.2 equiv), and DIPEA (1.5 equiv). The reaction was stirred overnight at room temperature and quenched by saturated $NaHCO_3$. DCM (50 mL) was added, and the organic layer was separated and dried. The solvent was removed under reduced pressure to afford the crude product that was purified by ISCO to give the desired products **22**−**23**.

*3′-(N-(3-(4-(2-(Dimethylamino)benzoyl)piperazin-1-yl)phenyl)-sulfamoyl)-4′-methoxy-N,N-dimethyl-[1,1′-biphenyl]-3-carboxa-mide (**22**).* Yield: 36% over three steps. $^1$H NMR (300 MHz, chloroform-*d*): $\delta$ 8.04 (d, $J$ = 2.07 Hz, 1H), 8.03 (d, $J_1$ = 9.0 Hz, $J_2$ = 177 Hz, 1H), 7.72 (d, $J$ = 8.67 Hz, 1H), 7.52 (d, $J$ = 12.06 Hz, 2H), 7.42 (t, $J$ = 7.54 Hz, 1H), 7.30−7.37 (m, 2H), 7.22 (d, $J$ = 7.16 Hz, 1H), 7.02−7.12 (m, 2H), 6.89−6.99 (m, 3H), 6.77 (s, 1H), 6.62 (d, $J$ = 8.10 Hz, 1H), 6.48 (d, $J$ = 7.54 Hz, 1H), 4.08 (s, 3H), 3.93 (br s, 1H), 3.84 (br s, 1H), 2.94−3.22 (m, 10H), 2.73−2.86 (m, 8H). MS (ESI) $m/z$: 642.2 $[M + H]^+$.

*4′-Methoxy-N,N-dimethyl-3′-(N-(3-(4-(3-methylbenzoyl)-piperazin-1-yl)phenyl)sulfamoyl)-[1,1′-biphenyl]-3-carboxamide (**23**).* Yield: 41% over three steps. $^1$H NMR (300 MHz, chloroform-*d*): $\delta$ 8.04 (d, $J$ = 2.26 Hz, 1H), 7.71 (dd, $J$ = 2.35, 8.57 Hz, 1H), 7.48−7.60 (m, 2H), 7.42 (t, $J$ = 7.54 Hz, 1H), 7.31−7.37 (m, 1H), 7.21−7.30 (m, 4H), 7.17 (d, $J$ = 7.16 Hz, 1H), 7.08 (d, $J$ = 8.85 Hz, 2H), 6.97−7.04 (m, 1H), 6.78 (s, 1H), 6.62 (d, $J$ = 8.29 Hz, 1H), 6.49 (d, $J$ = 7.72 Hz, 1H), 4.07 (s, 3H), 3.83 (br s, 2H), 3.54 (br s, 2H), 2.90−3.25 (m, 10H), 2.38 (s, 3H). MS (ESI) $m/z$: 613.2 $[M + H]^+$.

*N$^1$-(3-Nitrophenyl)ethane-1, 2-Diamine Hydrochloride (**61**).* Compound **45** was dissolved in minimum of ethyl acetate, and 4 N HCl in dioxane (50 mL) was added. The mixture was then stirred for 2 h until no bubbles were released. Hexane (100 mL) was added to precipitate any solid, and the suspension was filtered. The solid collected was rinsed with diethyl ether and dried in vacuum overnight to give the desired product. 17 g tan solid, yield: 78%. $^1$H NMR (300 MHz, DMSO-$d_6$): $\delta$ 8.12 (br s, 4H), 7.29−7.50 (m, 3H), 6.91−7.17 (m, 1H), 3.38 (t, $J$ = 6.40 Hz, 2H), 2.87−3.06 (m, 2H). MS (ESI) $m/z$: 182.2 $[M + H]^+$.

*N-(2-((3-Aminophenyl)amino)ethyl)-3-methylbenzamide (**63**).* 3-Methyl benzoic acid (2.73 g, 20 mmol) and 1,1′-carbonyldiimi-dazole (3.25 g, 20 mmol) were mixed in DCM and stirred for 15 min. Compound **59** (2.62 g, 10 mmol) was then added in one portion, followed by the addition of DIPEA (10.5 mL, 60 mmol). The reaction was then monitored by TLC. After completion, sat. $NaHCO_3$ was added to quench the reaction. The organic layer was then separated and dried by anhydrous $MgSO_4$. The solvent was removed under reduced pressure, and the residue (compound **62**) was then redissolved in the mixture of EtOH (80 mL) and water (30 mL), followed by the addition of ammonium chloride (10.7 g, 0.2 mol) and iron powder (7.84 g, 0.14 mol). The reaction was then brought to reflux for 2 h. After cooling down to room temperature, the reaction mixture was filtered and the filtrate was concentrated. Ethyl acetate (200 mL) and brine (200 mL) were added to the residue, and the organic layer was separated and dried. The solvent was removed under reduced pressure, and the residue was subjected to ISCO to give the desired product. 3.33 g, brown oil, yield: 62%. $^1$H NMR (300 MHz, DMSO-$d_6$): $\delta$ 8.56 (m, 2H), 7.54−8.22 (m, 3H), 7.10−7.50 (m, 2H), 7.02 (br s, 2H), 3.60−3.20 (m, 4H), 2.35 (s, 3H). MS (ESI) $m/z$: 270.2 $[M + H]^+$.

*N-(2-((3-((5-Bromo-2-methoxyphenyl)sulfonamido)phenyl)-amino)ethyl)-3-methylbenzamide (**64**).* Compound **63** (3.33 g, 12.4 mmol) was dissolved in DCM (100 mL) and triethylamine (3.5 mL, 24.7 mmol) was added, followed by the addition of catalytic DMAP (302 mg, 2.47 mmol). The mixture was then cooled to 0 °C, and 5-bromo-2-methoxy benzenesulfonyl chloride (3.86 g, 13.0 mmol) in THF (10 mL) was added slowly over a period of 20 min. The reaction was warmed up to room temperature and stirred overnight. The reaction was quenched by sat. $NaHCO_3$ (50 mL), and ethyl acetate (100 mL) was added. The organic layer was separated and dried. The solvent was removed under reduced pressure, and the residue was subjected to ISCO to give the desired product. 4.84 g, light-yellow foam, yield: 76%. $^1$H NMR (300 MHz, chloroform-*d*): $\delta$ 7.94 (d, $J$ = 2.45 Hz, 1H), 7.47−7.60 (m, 3H), 7.29−7.36 (m, 2H), 6.97 (t, $J$ = 8.01 Hz, 1H), 6.80−6.92 (m, 2H), 6.45 (d, $J$ = 2.07 Hz, 2H), 6.33−6.40 (m, 1H), 6.29 (d, $J$ = 9.23 Hz, 1H), 4.21 (br s, 1H), 4.00 (s, 3H), 3.66 (q, $J$ = 5.90 Hz, 2H), 3.32 (t, $J$ = 5.65 Hz, 2H), 2.39 (s, 3H). MS (ESI) $m/z$: 519.2 $[M + H]^+$.

**General Procedure for the Miyaura Borylation Reaction.** Aromatic bromides or iodides (1.0 equiv) were dissolved in 1,4-dioxane (0.1 M), and bis(pinacolato))diboron (1.5 equiv) was added, followed by $PdCl_2$(dppf) (0.1 equiv) and KOAc (2 equiv). The reaction was then heated at 90 °C overnight. After cooling to room temperature, the reaction mixture was filtered by Celite and the


https://doi.org/10.1021/acs.jmedchem.1c00841
J. Med. Chem. 2021, 64, 8806−8825

filtrate was concentrated under reduced pressure. The residue was subjected to ISCO to afford the desired product or used in the next Suzuki reaction without further purification.

**General Procedure for the Suzuki Coupling Reaction.** The boronic acid pinacol ester (1.0 equiv), aryl halide (1.0 equiv), and $K_2CO_3$ (2.0 equiv) were dissolved in a mixture of 1,4-dioxane and water (v/v = 4:1, 0.04 M). The mixture was degassed and purged with nitrogen three times. $Pd(PPh_3)_4$ (0.1 equiv) was then added, and the reaction was stirred at 90 °C for 1 h. The reaction was then cooled down and quenched with brine. Ethyl acetate was then added, and the organic layer was separated and dried. The solvent was removed under reduced pressure, and the residue was subjected to ISCO to give the pure desired product.

*N-(2-((3-((2-Methoxy-5-(4,4,5,5-tetramethyl-1,3,2-dioxaborolan-2-yl)phenyl)sulfonamido)p-henyl)amino)ethyl)-3-methylbenzamide (**65**).* **65** was prepared according to the general procedure for the Miyaura borylation reaction using compound **64** as the starting material. Yield: 87%. $^1$H NMR (300 MHz, chloroform-*d*): $\delta$ 8.29 (d, $J$ = 1.51 Hz, 1H), 8.15−8.27 (m, 1H), 7.85−7.95 (m, 1H), 7.45−7.65 (m, 2H), 7.28−7.34 (m, 2H), 6.89−7.00 (m, 3H), 6.84 (s, 1H), 6.20−6.53 (m, 3H), 4.10−4.22 (m, 1H), 4.03 (s, 3H), 3.64 (d, $J$ = 6.03 Hz, 2H), 3.33 (br s, 2H), 2.34−2.41 (m, 3H), 1.26−1.31 (m, 12H). MS (ESI) $m/z$: 566.2 $[M + H]^+$.

Compound **24**−**32** and **33**−**42** were prepared according to the general procedure for the Suzuki coupling reaction using compound **65** and the corresponding halogenated aromatic amide as starting materials.

*2-(4-Methoxy-3-(N-(3-((2-(3-methylbenzamido)ethyl)amino)-phenyl)sulfamoyl)phenyl)-N,N-dimethylisonicotinamide (**24**).* Yield:78%. $^1$H NMR (300 MHz, chloroform-*d*): $\delta$ 8.64 (d, $J$ = 4.90 Hz, 1H), 8.43 (d, $J$ = 2.45 Hz, 1H), 8.25 (dd, $J$ = 2.35, 8.76 Hz, 1H), 7.67 (s, 1H), 7.55 (s, 1H), 7.47 (d, $J$ = 6.59 Hz, 1H), 7.33−7.20 (m, 2H), 7.15 (dd, $J$ = 1.41, 4.99 Hz, 1H), 7.08 (d, $J$ = 8.85 Hz, 1H), 6.91−6.98 (m, 2H), 6.84−6.90 (m, 1H), 6.46−6.52 (m, 1H), 6.31 (d, $J$ = 8.10 Hz, 1H), 6.23 (d, $J$ = 9.04 Hz, 1H), 4.27−4.44 (m, 1H), 4.07 (s, 3H), 3.61 (d, $J$ = 5.46 Hz, 2H), 3.25 (t, $J$ = 5.56 Hz, 2H), 3.15 (s, 3H), 2.98 (s, 3H), 2.35 (s, 3H). MS (ESI) $m/z$: 588.2 $[M + H]^+$.

*5-(4-Methoxy-3-(N-(3-((2-(3-methylbenzamido)ethyl)amino)-phenyl)sulfamoyl)phenyl)-N,N-dimethylnicotinamide (**25**).* Yield: 80%. $^1$H NMR (300 MHz, chloroform-*d*): $\delta$ 8.78 (d, $J$ = 2.26 Hz, 1H), 8.60 (d, $J$ = 1.88 Hz, 1H), 8.08 (d, $J$ = 2.45 Hz, 1H), 7.89 (t, $J$ = 2.17 Hz, 1H), 7.70 (dd, $J$ = 2.45, 8.67 Hz, 1H), 7.57 (s, 1H), 7.50 (d, $J$ = 6.41 Hz, 1H), 7.09 (d, $J$ = 8.67 Hz, 1H), 6.95−7.03 (m, 1H), 6.86−6.95 (m, 1H), 6.46−6.51 (m, 1H), 6.34 (d, $J$ = 8.10 Hz, 1H), 6.25 (d, $J$ = 7.72 Hz, 1H), 4.07 (s, 3H), 3.60−3.70 (m, 2H), 3.26 (t, $J$ = 5.75 Hz, 2H), 3.15 (s, 3H), 3.06 (s, 3H), 2.35 (s, 3H). MS (ESI) $m/z$: 588.2 $[M + H]^+$.

*4-(4-Methoxy-3-(N-(3-((2-(3-methylbenzamido)ethyl)amino)-phenyl)sulfamoyl)phenyl)-N,N-dimethylpicolinamide (**26**).* Yield: 83%. $^1$H NMR (300 MHz, chloroform-*d*): $\delta$ 8.59 (d, $J$ = 5.27 Hz, 1H), 8.19 (d, $J$ = 2.26 Hz, 1H), 7.77 (d, $J$ = 2.07 Hz, 1H), 7.74 (d, $J$ = 2.45 Hz, 1H), 7.58 (s, 1H), 7.51 (d, $J$ = 6.41 Hz, 1H), 7.47 (dd, $J$ = 1.88, 5.27 Hz, 1H), 7.08 (d, $J$ = 8.67 Hz, 1H), 6.92 (t, $J$ = 8.01 Hz, 1H), 6.86 (s, 1H), 6.48 (s, 1H), 6.32 (d, $J$ = 8.29 Hz, 1H), 6.20 (d, $J$ = 9.23 Hz, 1H), 4.43−4.59 (m, 1H), 4.07 (s, 3H), 3.61−3.71 (m, 2H), 3.24 (t, $J$ = 5.56 Hz, 2H), 3.15 (d, $J$ = 3.58 Hz, 6H), 2.34 (s, 3H). MS (ESI) $m/z$: 588.1 $[M + H]^+$.

*6-(4-Methoxy-3-(N-(3-((2-(3-methylbenzamido)ethyl)amino)-phenyl)sulfamoyl)phenyl)-N,N-dimethylpicolinamide (**27**).* Yield: 85%. $^1$H NMR (300 MHz, chloroform-*d*): $\delta$ 8.58 (d, $J$ = 2.45 Hz, 1H), 8.15 (d, $J$ = 8.67 Hz, 1H), 7.77 (d, $J$ = 7.72 Hz, 1H), 7.70 (s, 1H), 7.56 (s, 1H), 7.48 (d, $J$ = 6.41 Hz, 2H), 7.06 (d, $J$ = 8.85 Hz, 1H), 6.86−6.98 (m, 1H), 6.82 (s, 2H), 6.46 (s, 1H), 6.21−6.35 (m, 2H), 4.28−4.44 (m, 1H), 4.06 (s, 3H), 3.57 (d, $J$ = 5.65 Hz, 2H), 3.22 (d, $J$ = 5.46 Hz, 2H), 3.17 (s, 3H), 3.11 (s, 3H), 2.37 (s, 3H). MS (ESI) $m/z$: 588.2 $[M + H]^+$.

*4-(4-Methoxy-3-(N-(3-((2-(3-methylbenzamido)ethyl)amino)-phenyl)sulfamoyl)phenyl)-N,N-dimethylthiophene-2-carboxamide (**28**).* Yield: 68%. $^1$H NMR (chloroform-*d*, 300 MHz): $\delta$ 8.01−8.04 (m, 1H), 7.62−7.68 (m, 1H), 7.55 (d, $J$ = 1.5 Hz, 2H), 7.47−7.52 (m, 1H), 7.45 (s, 1H), 7.30 (s, 2H), 7.00−7.05 (m, 1H), 6.91−6.99 (m, 1H), 6.79−6.83 (m, 1H), 6.58−6.66 (m, 1H), 6.46−6.50 (m, 1H), 6.31−6.37 (m, 1H), 6.24−6.30 (m, 1H), 4.21−4.34 (m, 1H), 4.05 (s, 3H), 3.25−3.33 (m, 2H), 3.10−3.24 (m, 2H), 2.38 ppm (s, 3H). MS (ESI) $m/z$: 593.1 $[M + H]^+$.

*5-(4-Methoxy-3-(N-(3-((2-(3-methylbenzamido)ethyl)amino)-phenyl)sulfamoyl)phenyl)-N,N-dimethylthiophene-3-carboxamide (**29**).* Yield: 88%. $^1$H NMR (300 MHz, chloroform-*d*): $\delta$ 8.08 (d, $J$ = 2.26 Hz, 1H), 7.64 (dd, $J_1$ = 2.35 Hz, $J_2$ = 8.57 Hz, 1H), 7.56 (s, 1H), 7.46−7.52 (m, 1H), 7.35 (s, 1H), 7.33−7.34 (m, 1H), 6.99 (d, $J$ = 8.67 Hz, 1H), 6.92 (d, $J$ = 8.29 Hz, 1H), 6.83−6.88 (m, 1H), 6.81 (s, 1H), 6.48 (s, 1H), 6.30−6.37 (m, 1H), 6.21−6.27 (m, 1H), 4.34−4.47 (m, 1H), 4.04 (s, 3H), 3.64 (d, $J$ = 5.84 Hz, 2H), 3.26 (s, 2H), 3.11 (br s, 6H), 2.37 (s, 3H). MS (ESI) $m/z$: 593.2 $[M + H]^+$.

*4-(4-Methoxy-3-(N-(3-((2-(3-methylbenzamido)ethyl)amino)-phenyl)sulfamoyl)phenyl)-N,N-dimethylthiazole-2-carboxamide (**30**).* Yield: 70%. $^1$H NMR (300 MHz, chloroform-*d*): $\delta$ 8.31 (d, $J$ = 2.26 Hz, 1H), 7.99−8.07 (m, 1H), 7.63−7.73 (m, 1H), 7.57 (s, 1H), 7.51−7.56 (m, 1H), 7.45−7.50 (m, 2H), 7.28−7.33 (m, 2H), 7.06 (d, $J$ = 8.67 Hz, 1H), 6.95 (m, 1H), 6.84 (s, 1H), 6.48 (s, 1H), 6.37−6.43 (m, 1H), 4.08 (s, 3H), 3.57−3.67 (m, 5H), 3.24−3.33 (m, 2H), 3.17 (s, 3H), 2.38 (s, 3H). MS (ESI) $m/z$: 594.2 $[M + H]^+$.

*(E)-N-(2-((3-((5-(3-(Dimethylamino)-3-oxoprop-1-en-1-yl)-2-methoxyphenyl)sulfonamido)-phenyl)amino)ethyl)-3-methylbenzamide (**31**).* Yield: 63%. $^1$H NMR (300 MHz, chloroform-*d*): $\delta$ 8.03 (d, $J$ = 2.26 Hz, 1H), 7.46−7.59 (m, 5H), 7.28−7.34 (m, 2H), 6.91−7.01 (m, 2H), 6.73−6.85 (m, 2H), 6.50−6.58 (m, 1H), 6.44 (s, 1H), 6.24−6.38 (m, 2H), 4.13−4.32 (m, 1H), 4.04 (s, 3H), 3.65 (d, $J$ = 5.84 Hz, 2H), 3.29 (s, 2H), 3.14 (s, 3H), 3.04 (s, 3H), 2.39 (s, 3H). MS (ESI) $m/z$: 537.2 $[M + H]^+$.

*N-(2-((3-((5-(3-(Dimethylamino)-3-oxopropyl)-2-methoxyphenyl)sulfonamido)phenyl)amino)ethyl)-3-methylbenzamide (**32**).* Yield: 67%. $^1$H NMR (300 MHz, chloroform-*d*): $\delta$ 7.64 (d, $J$ = 2.26 Hz, 1H), 7.58 (s, 1H), 7.52 (br s, 1H), 7.28−7.36 (m, 3H), 6.95 (t, $J$ = 8.01 Hz, 1H), 6.89 (d, $J$ = 8.29 Hz, 1H), 6.83 (s, 1H), 6.67−6.75 (m, 1H), 6.43 (s, 1H), 6.35 (s, 1H), 6.28 (d, $J$ = 7.54 Hz, 1H), 3.98 (s, 3H), 3.64 (d, $J$ = 5.65 Hz, 2H), 3.30 (t, $J$ = 5.75 Hz, 2H), 2.81−2.92 (m, 8H), 2.49−2.57 (m, 2H), 2.39 (s, 3H). MS (ESI) $m/z$: 539.2 $[M + H]^+$.

*N-(2-(Dimethylamino)ethyl)-4′-methoxy-N-methyl-3′-(N-(3-((2-(3-methylbenzamido)ethyl)amino)phenyl)sulfamoyl)-[1,1′-biphenyl]-3-carboxamide (**33**).* Yield: 72%. $^1$H NMR (300 MHz, chloroform-*d*): $\delta$ 8.12 (d, $J$ = 2.26 Hz, 1H), 7.69 (dd, $J_1$ = 2.35 Hz, $J_2$ = 8.57 Hz, 1H), 7.58 (br s, 3H), 7.53 (s, 2H), 7.38−7.47 (m, 2H), 7.30−7.37 (m, 2H), 7.15 (br s, 2H), 7.04 (d, $J$ = 8.67 Hz, 1H), 6.93 (t, $J$ = 8.01 Hz, 2H), 6.46 (s, 1H), 6.32 (d, $J$ = 7.91 Hz, 1H), 6.23 (d, $J$ = 9.23 Hz, 1H), 4.04 (s, 3H), 3.65−3.74 (m, 1H), 3.55−3.64 (m, 2H), 3.31−3.42 (m, 1H), 3.17−3.26 (m, 2H), 3.11 (br s, 1H), 3.04 (br s, 2H), 2.61−2.71 (m, 1H), 2.41−2.50 (m, 1H), 2.34 (s, 6H), 2.08 (br s, 3H). MS (ESI) $m/z$: 644.2 $[M + H]^+$.

*N-(2-(Dimethylamino)ethyl)-4′-methoxy-3′-(N-(3-((2-(3-methylbenzamido)ethyl)amino)phe-nyl)sulfamoyl)-[1,1′-biphenyl]-3-carboxamide (**34**).* Yield: 75%. $^1$H NMR (300 MHz, chloroform-*d*): $\delta$ 8.14 (d, $J$ = 2.45 Hz, 1H), 8.02 (s, 1H), 7.78−7.84 (m, 1H), 7.66−7.73 (m, 2H), 7.63 (s, 1H), 7.55 (br s, 2H), 7.49 (d, $J$ = 3.20 Hz, 2H), 7.20 (br s, 2H), 7.04 (d, $J$ = 8.67 Hz, 1H), 6.93 (t, $J$ = 7.91 Hz, 2H), 6.55 (s, 1H), 6.31 (d, $J$ = 8.10 Hz, 1H), 6.23 (d, $J$ = 6.22 Hz, 1H), 4.03 (s, 3H), 3.65 (d, $J$ = 5.65 Hz, 2H), 3.47−3.58 (m, 2H), 3.26 (br s, 2H), 2.57 (t, $J$ = 5.75 Hz, 1H), 2.52 (d, $J$ = 6.03 Hz, 1H), 2.31 (s, 6H), 2.25 (s, 3H). MS (ESI) $m/z$: 630.2 $[M + H]^+$; LCMS.

*4′-Methoxy-N-methyl-3′-(N-(3-((2-(3-methylbenzamido)ethyl)-amino)phenyl)sulfamoyl)-N-(pyridin-2-yl)-[1,1′-biphenyl]-3-carboxamide (**35**).* Yield: 78%. $^1$H NMR (300 MHz, chloroform-*d*): $\delta$ 8.36−8.40 (m, 1H), 8.24−8.33 (m, 2H), 8.18−8.22 (m, 1H), 7.70−7.76 (m, 1H), 7.59−7.62 (m, 1H), 7.56−7.59 (m, 1H), 7.53−7.56 (m, 1H), 7.50−7.52 (m, 1H), 7.47−7.50 (m, 1H), 7.44−7.47 (m, 1H), 7.30−7.39 (m, 2H), 7.21 (s, 1H), 7.18 (s, 1H), 7.02−7.07 (m, 1H), 6.89−6.96 (m, 1H), 6.79−6.83 (m, 1H), 6.49−6.58 (m, 2H), 6.27−6.33 (m, 1H), 6.14−6.22 (m, 1H), 4.04 (s, 3H), 3.90 (s, 3H), 3.63−3.73 (m, 2H), 3.23−3.35 (m, 2H), 2.28 (s, 3H). MS (ESI) $m/z$: 650.2 $[M + H]^+$.


https://doi.org/10.1021/acs.jmedchem.1c00841
J. Med. Chem. 2021, 64, 8806−8825

*N-Benzyl-4′-methoxy-N-methyl-3′-(N-(3-((2-(3-methylbenzamido)ethyl)amino)phenyl)sulfamoyl)-[1,1′-biphenyl]-3-carboxamide (**36**).* Yield: 81%. $^1$H NMR (300 MHz, chloroform-*d*): δ 8.13 (br s, 1H), 7.48−7.75 (m, 5H), 7.30−7.46 (m, 6H), 6.99−7.21 (m, 3H), 6.93 (t, *J* = 7.91 Hz, 1H), 6.85 (s, 1H), 6.45 (s, 1H), 6.32 (d, *J* = 8.10 Hz, 1H), 6.23 (d, *J* = 7.72 Hz, 1H), 4.49−4.82 (m, 2H), 4.04 (s, 3H), 3.58 (br s, 2H), 3.21 (br s, 2H), 2.76−3.11 (m, 3H), 2.33 (br s, 3H). MS (ESI) *m*/*z*: 663.2 [M + H]$^+$.

*4′-Methoxy-N-methyl-3′-(N-(3-((2-(3-methylbenzamido)ethyl)amino)phenyl)sulfamoyl)-N-(-pyridin-2-ylmethyl)-[1,1′-biphenyl]-3-carboxamide (**37**).* Yield: 84%. $^1$H NMR (300 MHz, chloroform-*d*): δ 8.56−8.69 (m, 1H), 8.00−8.17 (m, 1H), 7.67−7.77 (m, 2H), 7.47−7.66 (m, 5H), 7.42 (br s, 3H), 7.01−7.13 (m, 2H), 6.93 (t, *J* = 8.01 Hz, 1H), 6.84 (br s, 1H), 6.46 (s, 1H), 6.32 (d, *J* = 8.10 Hz, 1H), 6.17−6.27 (m, 1H), 4.88 (s, 1H), 4.62 (s, 1H), 4.04 (br s, 3H), 3.59 (br s, 2H), 3.21 (br s, 2H), 3.09 (d, *J* = 15.82 Hz, 3H), 2.34 (br s, 3H). MS (ESI) *m*/*z*: 664.2 [M + H]$^+$.

*4′-Methoxy-3′-(N-(3-((2-(3-methylbenzamido)ethyl)amino)phenyl)sulfamoyl)-N-(pyridin-2-ylmethyl)-[1,1′-biphenyl]-3-carboxamide (**38**).* Yield: 62%. $^1$H NMR (300 MHz, chloroform-*d*): δ 8.52−8.60 (m, 1H), 8.14 (d, *J* = 2.45 Hz, 1H), 8.04 (s, 1H), 7.78 (d, *J* = 7.72 Hz, 2H), 7.61−7.72 (m, 3H), 7.44−7.56 (m, 3H), 7.06−7.14 (m, 1H), 6.98−7.05 (m, 2H), 6.88−6.98 (m, 1H), 6.55 (s, 1H), 6.27−6.36 (m, 1H), 6.19−6.26 (m, 1H), 4.72 (d, *J* = 4.90 Hz, 2H), 4.25−4.48 (m, 1H), 4.00 (s, 3H), 3.65 (d, *J* = 5.46 Hz, 2H), 3.29 (br s, 2H), 2.30 (s, 3H). MS (ESI) *m*/*z*: 650.2 [M + H]$^+$.

*4′-Methoxy-N-methyl-3′-(N-(3-((2-(3-methylbenzamido)ethyl)amino)phenyl)sulfamoyl)-N-(pyridin-3-ylmethyl)-[1,1′-biphenyl]-3-carboxamide (**39**).* Yield: 68%. $^1$H NMR (300 MHz, methanol-$d_4$): δ 8.40−8.62 (m, 1H), 7.86−8.07 (m, 1H), 7.31 (s, 12H), 7.10−7.23 (m, 1H), 6.84−6.92 (m, 1H), 6.45−6.51 (m, 1H), 6.35−6.42 (m, 1H), 6.24−6.35 (m, 1H), 3.99 (s, 3H), 3.40−3.48 (m, 2H), 3.21 (m, 2H), 2.94−3.08 (m, 3H), 2.36 (s, 3H). MS (ESI) *m*/*z*: 664.1 [M + H]$^+$.

*4′-Methoxy-N-methyl-3′-(N-(3-((2-(3-methylbenzamido)ethyl)amino)phenyl)sulfamoyl)-N-(pyridin-4-ylmethyl)-[1,1′-biphenyl]-3-carboxamide (**40**).* Yield: 80%. $^1$H NMR (300 MHz, methanol-$d_4$): δ 8.49 (br s, 2H), 7.91−8.09 (m, 1H), 7.02−7.78 (m, 12H), 6.86 (t, *J* = 8.10 Hz, 1H), 6.50 (br s, 1H), 6.40 (d, *J* = 6.59 Hz, 1H), 6.23−6.33 (m, 1H), 4.49−4.83 (m, 2H), 3.95 (br s, 3H), 3.36−3.49 (m, 2H), 3.18 (t, *J* = 6.03 Hz, 2H), 2.89−3.10 (m, 3H), 2.33 (s, 3H). $^{13}$C NMR (75 MHz, chloroform-*d*): δ 174.1 (1C, *J* = 45 Hz), 170.7, 157.9, 150.7, 150.5, 148.9, 141.0, 139.8, 139.5, 137.6, 135.6, 134.3, 133.3, 130.6, 130.4, 130.2, 129.5, 129.3, 128.8, 128.5, 126.9, 126.4, 126.2, 125.8, 125.4, 124.3, 123.4, 114.2, 110.5, 110.2, 105.6, 56.9, 53.3 (1 C, *J* = 307.5 Hz), 44.1, 40.4, 36.4 (1C, *J* = 307.5 Hz), 21.4. MS (ESI) *m*/*z*: 664.2 [M + H]$^+$.

*4′-Methoxy-N-methyl-3′-(N-(3-((2-(3-methylbenzamido)ethyl)amino)phenyl)sulfamoyl)-N-(2-(pyridin-2-yl)ethyl)-[1,1′-biphenyl]-3-carboxamide (**41**).* Yield: 85%. $^1$H NMR (300 MHz, methanol-$d_4$): δ 8.25 (dd, $J_1$ = 159.0 Hz, $J_2$ = 3.0 Hz, 1H), 7.95 (d, *J* = 33.0 Hz, 1H), 7.73−7.84 (m, 1H), 7.58 (dd, $J_1$ = 63.0 Hz, $J_2$ = 9.0 Hz, 1H), 7.18−7.62 (m, 9H), 7.03 (t, *J* = 6.0 Hz, 1H), 6.91 (t, *J* = 6.0 Hz, 1H), 6.48−6.83 (m, 2H), 6.42 (t, *J* = 9.0 Hz, 1H), 6.26−6.36 (m, 1H), 4.03 (d, *J* = 12.0 Hz, 3H), 3.91 (t, *J* = 6.0 Hz, 1H), 3.71 (t, *J* = 6.0 Hz, 1H), 3.35−3.58 (m, 2H), 3.08−3025 (m, 7H), 2.37 (s, 3H). MS (ESI) *m*/*z*: 678.2 [M + H]$^+$.

*4′-Methoxy-N-methyl-3′-(N-(3-((2-(3-methylbenzamido)ethyl)amino)phenyl)sulfamoyl)-N-(2-(pyridin-4-yl)ethyl)-[1,1′-biphenyl]-3-carboxamide (**42**).* Yield: 70%. $^1$H NMR (300 MHz, chloroform-*d*): δ 8.55 (br s, 1H), 8.25−8.36 (m, 1H), 7.95−8.11 (m, 1H), 7.30−7.75 (m, 6H), 6.68−7.22 (m, 8H), 6.49 (br s, 1H), 6.31 (br s, 2H), 4.04 (s, 3H), 3.83 (br s, 1H), 3.59 (br s, 4H), 3.12−3.29 (m, 3H), 3.03 (br s, 1H), 2.90 (br s, 3H), 2.34 (s, 3H). MS (ESI) *m*/*z*: 678.1 [M + H]$^+$.

**General Procedure for the Synthesis of Compounds 43 and 44.** Intermediate **63** (539 mg, 2.0 mmol) was dissolved in DCM (20 mL), and triethylamine (0.56 mL, 4.0 mmol) was added. Then, catalytic DMAP (25 mg, 0.4 mmol) was introduced and the reaction mixture was cooled down to 0 °C. At this temperature, 5-bromo-2-methoxybenzenecarboxylic chloride (499 mg, 2.0 mmol) in THF (10 mL) was added slowly. The reaction was then stirred at this temperature for 1 h and allowed to warm up to room temperature overnight. Saturated sodium bicarbonate (50 mL) was added to quench the reaction, and the reaction was extracted with ethyl acetate (50 mL). The organic layer was separated and dried. The solvent was removed under reduced pressure, and the residue was subjected to ISCO to give the desired product **66**.

*5-Bromo-2-methoxy-N-[3-({2-[(3-methylphenyl)formamido]-ethyl}amino)phenyl]benzamide (**66**).* 579 mg, yield: 60%. $^1$H NMR (300 MHz, chloroform-*d*): δ 9.61 (s, 1H), 8.35 (d, *J* = 2.64 Hz, 1H), 7.47−7.62 (m, 3H), 7.21−7.35 (m, 4H), 7.12 (t, *J* = 8.01 Hz, 1H), 6.90 (d, *J* = 8.85 Hz, 1H), 6.75 (d, *J* = 7.91 Hz, 1H), 6.65 (br s, 1H), 6.43 (dd, *J* = 1.70, 8.10 Hz, 1H), 4.15−4.27 (m, 1H), 4.02 (s, 3H), 3.69 (q, *J* = 5.97 Hz, 2H), 3.32−3.50 (m, 2H), 2.36 (s, 3H). MS (ESI) *m*/*z*: 484.2 [M + H]$^+$.

Compound **67** was synthesized according to the general procedure for the Miyaura borylation reaction using **66** as the starting material. Yield: >99%.

*2-Methoxy-N-[3-({2-[(3-methylphenyl)formamido]ethyl}amino)-phenyl]-5-(tetramethyl-1,3-,2-dioxaborolan-2-yl)benzamide (**67**).* Yield: > 99%. $^1$H NMR (300 MHz, chloroform-*d*): δ 9.57 (s, 1H), 8.70 (d, *J* = 1.51 Hz, 1H), 7.91 (dd, *J* = 1.60, 8.19 Hz, 1H), 7.51−7.66 (m, 2H), 7.42 (s, 1H), 7.22−7.35 (m, 3H), 7.12 (t, *J* = 8.01 Hz, 1H), 7.01 (d, *J* = 8.29 Hz, 1H), 6.73 (d, *J* = 7.91 Hz, 1H), 6.63 (br s, 1H), 6.44 (d, *J* = 7.91 Hz, 1H), 4.05 (s, 3H), 3.72 (q, *J* = 5.65 Hz, 2H), 3.37−3.52 (m, 2H), 2.37 (s, 3H), 1.33 (s, 12H). MS (ESI) *m*/*z*: 530.2 [M + H]$^+$.

Compounds **43** and **44** were synthesized according to the general procedure for the Suzuki coupling reaction using compound **67** as the starting material.

*4-Methoxy-N$^{3′}$,N$^{3′}$-dimethyl-N$^3$-(3-((2-(3-methylbenzamido)-ethyl)amino)phenyl)-[1,1′-biphenyl]-3,3′-dicarboxamide (**43**).* Yield: 78%. $^1$H NMR (300 MHz, chloroform-*d*): δ 9.77 (s, 1H), 8.53 (d, *J* = 2.26 Hz, 1H), 7.73 (dd, *J* = 2.45, 8.48 Hz, 1H), 7.66 (s, 2H), 7.58 (s, 1H), 7.54 (br s, 1H), 7.47 (t, *J* = 7.91 Hz, 1H), 7.34−7.42 (m, 3H), 7.29 (d, *J* = 4.71 Hz, 2H), 7.09−7.21 (m, 3H), 6.79 (d, *J* = 8.48 Hz, 1H), 6.46 (d, *J* = 8.10 Hz, 2H), 4.13−4.22 (m, 1H), 4.10 (s, 3H), 3.68−3.78 (m, 2H), 3.47 (t, *J* = 5.75 Hz, 3H), 2.93−3.19 (m, 7H), 2.38 (s, 3H). MS (ESI) *m*/*z*: 551.2 [M + H.

*4-Methoxy-N$^{3′}$-methyl-N$^3$-(3-((2-(3-methylbenzamido)ethyl)-amino)phenyl)-N$^{3′}$-(yridine-4-ylmethyl)-[1,1′-biphenyl]-3,3′-dicarboxamide (**44**).* Yield: 72%. $^1$H NMR (300 MHz, chloroform-*d*): δ 9.75 (br s, 1H), 8.62 (d, *J* = 6.03 Hz, 2H), 8.40−8.57 (m, 1H), 7.69 (d, *J* = 7.72 Hz, 3H), 7.36−7.60 (m, 5H), 7.28−7.34 (m, 3H), 7.06−7.22 (m, 3H), 6.72−6.83 (m, 1H), 6.46 (d, *J* = 7.91 Hz, 1H), 4.78 (br s, 2H), 4.10 (s, 3H), 3.74 (q, *J* = 5.84 Hz, 2H), 3.41−3.53 (m, 2H), 2.90−3.16 (m, 3H), 2.37 (s, 3H). MS (ESI) *m*/*z*: 628.2 [M + H]$^+$.

**OX1R and OX2R Calcium Mobilization Assays.** Activity of the target compounds at the human $OX_1$ and $OX_2$ receptors was determined utilizing CHO RD-HGA16 cells (Molecular Devices) engineered to stably express either the human $OX_1$ or the human $OX_2$ receptor. Cells were maintained in Ham's F12 supplemented with 10% fetal bovine serum, 100 units of penicillin and streptomycin, and 100 μg/mL normocin. To conduct the assay, cells were plated at 25,000 cells/well into 96-well black-wall/clear-bottom assay plates and incubated overnight at 37 °C, 5% $CO_2$. The next day prior to the assay, Calcium 5 dye (Molecular Devices) was reconstituted according to the manufacturer's instructions. The reconstituted dye was diluted 1:40 in prewarmed (37 °C) assay buffer (1× Hank's balanced salt solution, 20 mM 4-(2-hydroxyethyl)-1-piperazineethanesulfonic acid, 2.5 mM probenecid, pH 7.4 at 37 °C). Growth medium was removed and the cells were gently washed with 100 μL of prewarmed (37 °C) assay buffer. The cells were incubated for 45 min at 37 °C, 5% $CO_2$ in 200 μL of the diluted Calcium 5 dye. Serial dilutions of test compounds and the agonist control orexin A were prepared at 10x the desired final concentration in 0.25% bovine serum albumin/1% dimethyl sulfoxide (DMSO)/assay buffer, aliquoted into 96-well polypropylene plates and warmed to 37 °C for 15 min. After the dye-loading incubation period, cells were pretreated with 25 μL of 9% DMSO/assay buffer and incubated for 15 min at 37 °C. After the


https://doi.org/10.1021/acs.jmedchem.1c00841
J. Med. Chem. 2021, 64, 8806−8825

pretreatment incubation period, the plate was read with a FlexStation II (Molecular Devices). Calcium-mediated changes in fluorescence were monitored every 1.52 s over a 60 s time period, with the FlexStation II adding 25 μL of the test compound/control serial dilutions at the 19 s time point (excitation at 485 nm, detection at 525 nm). Peak kinetic reduction (SoftMax, Molecular Devices) relative fluorescent units were plotted against the log of compound concentration, and nonlinear regression analysis was used to generate $EC_{50}$ values (GraphPad Prism, GraphPad Software, Inc., San Diego, CA).

**Computational Methods.** *Preparation of Initial Full-Length OX2R and OX1R Models.* Initial full-length models of human OX2R were prepared based on the reported coordinates for **5** (PDBID: 7L1V) and orexin-B-bound OX2R (PDBID: 7L1U) cryo-EM structures,[50] with restoration of missing residues in loops and reversal of truncation of ICL3 and the N- and C-termini. In addition, the miniGsqi/Gβ1γ2 segments that were absent in the **5** and orexin-B-bound cryogenic structural solutions were completed using MODELLER.[61] Thus, the initial conformations of the ICL3/N- and C-termini of the OX2R were generated self-consistently with the initial full-length G-protein. To accomplish these steps, a sequence alignment between the sequence present in the cryogenic construct and the human OX2R sequence was performed, employing CLUSTALX[74] and a GONNET 250 scoring matrix and a GAP penalty of 10. This sequence and the cryogenic coordinates of OX2R were input to MODELLER and the best zDOPE scored models collected to select the top scored model for input into SCWRL,[75] where new (nonclashing) rotameric states of nonconserved residues were generated for the newly modeled residues. We then employed the Epik function embodied in the Schrodinger small-molecule suite to make self-consistent protonation assignments along with Schrodinger protein preparation steps. The model was then energy minimized for 2500 conjugate gradients (PBCG) steps following implementation of a disulfide constraint between cysteine127 and cysteine210. The completed model then underwent nudged elastic band pulls of the N-/C-termini to generate compact initial coordinates (primarily to move away from fully extended initial N-/C-terminal conformations) and the full model immersed in an initial 200 × 200 × 200 $Å^3$ 1,2-dioleoyl-*sn*-glycero-3-phosphocholine (DOPC) lipid box with 50 Å layer of water/KCl above and below the lipid bilayer. The system was then parameterized using the AMBER LIPD14[65] and the AMBER18[76] ffSB14 force fields including TIP3P model parameters. The initial simulation membrane system/GPCR complex was obtained by immersing the GPCR complex (excluding the G-protein portion for this study) in the membrane/water/ion system and deleting all lipids/water/ions within 3.5 Å of any GPCR-complex atom. The system was then energy minimized using 8000 steps of AMBER sander conjugate gradient steps, heated with all atoms constrained for 5 ns and then equilibrated unconstrained for ca. 30 ns. In the case of **40**, we continued with production MD out to 180 ns using AMBER (particle mesh Ewald MD) for the purpose of examining time-dependent interactions between the Schrodinger-induced fit poses and residues in the orthosteric binding site.

*Docking, Induced Fit, and MD Studies.* The initial full-length models following equilibration and energy minimization were employed in GLIDE SP/XP and induced-fit studies. Our docking protocol was to collect 120 post docking energy-minimized poses, which were then distilled to the top five poses. We found simple GLIDE SP/XP docking with a rigid receptor was often inadequate to get good self-docking (i.e., docking the native ligand from the crystal or cryo-EM structures) with GPCRs such as OX1R and OX2R, which is often improved with introduction of receptor flexibility. To his end, we employed MODELLER annealing of initial cryogenic structural solution coordinates and verified adequate docking and root-mean-square deviations (RMSD's) using GLIDE SP, which has a more exhaustive configuration sampling than GLIDE-XP which uses a more conservative anchor and grow (CONFGEN[77]) sampling approach. A simple GLIDE-SP docking of **5** in the OX2R gave a RMSD of 2.5 Å for the best Emodel scored pose, demonstrating structural similarity to the cryo-EM structures and adequate pose reproduction. In all remaining cases, we employed induced fit and/or MD equilibration starting with initial GLIDE-XP poses. The top Emodel docked pose was then used as the seed structure for Schrodinger-Prime induced-fit modeling with a flexibility of 5−7 Å around any atom in the ligand. We used the 7 Å extended region, in particular, to include Arg and Lys residues at the top of the OX2R and OX1R full-length models and explicitly included $R339^{7.28}$ (OX2R) and $R333^{7.29}$ (OX1R) in order to enhance sampling of variable conformations including those residues in GLIDE-XP redocking into the Prime variable backbone/sidechain conformation sampled OX2R and OX1R configurations in an induced-fit procedure.[78] Top scoring induced fit poses were then analyzed for salient interactions, and these were employed in following MD studies. All ligand models for use in Schrodinger GLIDE SP/XP docking were prepared with the LIGPREP module.

**Sleep Studies.** *Animals.* Twelve-month-old male mice (bred at Minneapolis VA Health Care System, $n = 6$) were housed individually in solid-bottom cages with corncob bedding and a chewing substrate (Nylabone, natural flavor, BioServ, Frenchtown, NJ). Throughout the study, a 12 h light/12 h dark cycle (lights on at 06:00) in a temperature-controlled environment (21−22 °C) was used for experiments. Rodent chow (Harlan Teklad 8604) and water were allowed ad libitum. Studies were approved by the Institutional Animal Care and Use Committee at the Minneapolis VA Health Care System.

*Surgery.* Mice were anesthetized with a ketamine/xylazine mixture (15 mg/kg; 1.5 mg/kg) and implanted with a radiotelemetric transmitter and EEG/EMG electrodes to record vigilance states (F20-EET, Data Sciences International [DSI], St. Paul, MN). Stereotaxic coordinates for the EE electrodes were as follows: −0.1 mm anterior, 2.0 mm lateral to bregma, and inserted to predrilled holes to touch the dura. The EMG leads were secured in the nuchal musculature. Animals were allowed to recover from surgery for at least 7−10 days before experimental trials began.

*Injections.* Mice were injected with either **40** (RTOXA-43, 40 mg/kg i.p. in 0.3 mL saline) or vehicle (saline, $n = 5$) in a counterbalanced design. Doses were chosen based on results from sleep studies on YNT-185.[46] Mice were randomly assigned to a treatment group; each animal received each treatment once, and all treatments were represented on each day. Injections were performed between 10:00 and 10:30 (zeitgeber time 4−4.5) with ≥48 h between treatments. Continuous EEG/EMG recordings were obtained for 24 h postinjection.

*EEG/EMG Recording and Behavioral-State Determination.* To allow freely moving polysomnogram recordings, a receiver (PhysioTel RPC-1, DSI, St. Paul, MN) was placed beneath the testing cage to detect EEG/EMG signals from the implanted transmitter. Briefly, signals were digitized by a Data Exchange Matrix connected to a PC with Dataquest A.R.T 4.1 software (DSI, St. Paul, MN). Electroencephalogram signals (0.3−30.0 Hz band pass) and EMG signals (1.0−100.0 Hz bandpass) were stored on a computer, visualized with Neuroscore software (version 2.0.1, DSI, St. Paul, MN), and sleep and wakefulness states were scored manually in accordance with previously described methods. In brief, consecutive 10 s epochs of EEG and EMG signals were classified into one of the following three behavioral states: NREM sleep, REM sleep, or wakefulness, and percent time spent in each state was then calculated from the scored data. The following dependent variables were quantified for each recording session: (a) percent time spent in wakefulness, NREM sleep, REM sleep; (b) total number of episodes for each vigilance state; (c) mean duration of episodes for each vigilance state; and (d) total number of state transitions.

## ■ ASSOCIATED CONTENT

### Supporting Information

The Supporting Information is available free of charge at https://pubs.acs.org/doi/10.1021/acs.jmedchem.1c00841.

HPLC analysis results of target compounds and summary table of molecular formula strings with biological data (PDF)



https://doi.org/10.1021/acs.jmedchem.1c00841
J. Med. Chem. 2021, 64, 8806−8825

Molecular strings for the target compounds (CSV)

Coordinates for OX1R model (PDB)

Coordinates for OX2R model (PDB)

## AUTHOR INFORMATION


### Corresponding Author

**Yanan Zhang** − *Research Triangle Institute, Research Triangle Park, North Carolina 27709, United States;* orcid.org/0000-0001-7153-4358; Phone: 1-919-541-1235; Email: yzhang@rti.org; Fax: 1-919-541-6499

### Authors

**Dehui Zhang** − *Research Triangle Institute, Research Triangle Park, North Carolina 27709, United States*

**David A. Perrey** − *Research Triangle Institute, Research Triangle Park, North Carolina 27709, United States*

**Ann M. Decker** − *Research Triangle Institute, Research Triangle Park, North Carolina 27709, United States*

**Tiffany L. Langston** − *Research Triangle Institute, Research Triangle Park, North Carolina 27709, United States*

**Vijayakumar Mavanji** − *Research Service, Veterans Affairs Health Care System, Minneapolis, Minnesota 55417, United States*

**Danni L. Harris** − *Research Triangle Institute, Research Triangle Park, North Carolina 27709, United States*

**Catherine M. Kotz** − *Research Service, Veterans Affairs Health Care System, Minneapolis, Minnesota 55417, United States; Department of Integrative Biology and Physiology, University of Minnesota, Minneapolis, Minnesota 55455, United States; Geriatric, Research, Education and Clinical Center, Minneapolis Veterans Affairs Health Care System, Minneapolis, Minnesota 55417, United States*

Complete contact information is available at: https://pubs.acs.org/10.1021/acs.jmedchem.1c00841


### Author Contributions

The manuscript was written through contributions of all authors. All authors have given approval to the final version of the manuscript. We thank Emma Tonetti for technical assistance.


### Funding

This work was supported by the National Institute on Drug Abuse, the National Institutes of Health, U.S. (grants DA040693 to Y.Z.), and the US Department of Veteran Affairs (grants 1IO1BX003004-01A2 and 1IO1BX003687-01A1 to C.M.K.).


### Notes

The authors declare no competing financial interest.

## ABBREVIATIONS

1,2-DCE, 1,2-dichloroethane; DCM, dichloromethane; DME, 1,2-dimethoxyethane; DOPC, 1,2-dioleoyl-*sn*-glycero-3-phosphocholine; $EC_{50}$, half-maximal effective concentration; FLIPR, fluorometric imaging plate reader; GPCR, G protein-coupled receptor; HPLC, high-performance liquid chromatography; KCl, potassium chloride; MD, molecular dynamics; MS, mass spectrometry; NMR, nuclear magnetic resonance; OX1R, orexin-1 receptor; OX2R, orexin-2 receptor; RMSD, root-mean-square deviation; SAR, structure−activity relationship; TLC, thin-layer chromatography

## REFERENCES


(1) de Lecea, L.; Kilduff, T. S.; Peyron, C.; Gao, X. B.; Foye, P. E.; Danielson, P. E.; Fukuhara, C.; Battenberg, E. L. F.; Gautvik, V. T.; Bartlett, F. S., II; Frankel, W. N.; van den Pol, A. N.; Bloom, F. E.; Gautvik, K. M.; Sutcliffe, J. G. The hypocretins: Hypothalamus-specific peptides with neuroexcitatory activity. *Proc. Natl. Acad. Sci. U.S.A.* **1998**, *95*, 322−327.

(2) Sakurai, T.; Amemiya, A.; Ishii, M.; Matsuzaki, I.; Chemelli, R. M.; Tanaka, H.; Williams, S. C.; Richardson, J. A.; Kozlowski, G. P.; Wilson, S.; Arch, J. R. S.; Buckingham, R. E.; Haynes, A. C.; Carr, S. A.; Annan, R. S.; McNulty, D. E.; Liu, W.-S.; Terrett, J. A.; Elshourbagy, N. A.; Bergsma, D. J.; Yanagisawa, M. Orexins and orexin receptors: A family of hypothalamic neuropeptides and g protein-coupled receptors that regulate feeding behavior. *Cell* **1998**, *92*, 573−585.

(3) Peyron, C.; Tighe, D. K.; van den Pol, A. N.; de Lecea, L.; Heller, H. C.; Sutcliffe, J. G.; Kilduff, T. S. Neurons containing hypocretin (orexin) project to multiple neuronal systems. *J. Neurosci.* **1998**, *18*, 9996−10015.

(4) Date, Y.; Ueta, Y.; Yamashita, H.; Yamaguchi, H.; Matsukura, S.; Kangawa, K.; Sakurai, T.; Yanagisawa, M.; Nakazato, M. Orexins, orexigenic hypothalamic peptides, interact with autonomic, neuroendocrine and neuroregulatory systems. *Proc. Natl. Acad. Sci. U.S.A.* **1999**, *96*, 748−753.

(5) Nambu, T.; Sakurai, T.; Mizukami, K.; Hosoya, Y.; Yanagisawa, M.; Goto, K. Distribution of orexin neurons in the adult rat brain. *Brain Res.* **1999**, *827*, 243−260.

(6) Sutcliffe, J. G.; de Lecea, L. The hypocretins: Setting the arousal threshold. *Nat. Rev. Neurosci.* **2002**, *3*, 339−348.

(7) Sakurai, T. Roles of orexin/hypocretin in regulation of sleep/wakefulness and energy homeostasis. *Sleep Med. Rev.* **2005**, *9*, 231−241.

(8) de Lecea, L.; Sutcliffe, J. G. The hypocretins and sleep. *FEBS J.* **2005**, *272*, 5675−5688.

(9) Kilduff, T. S.; Peyron, C. The hypocretin/orexin ligand-receptor system: Implications for sleep and sleep disorders. *Trends Neurosci.* **2000**, *23*, 359−365.

(10) Ohno, K.; Sakurai, T. Orexin neuronal circuitry: Role in the regulation of sleep and wakefulness. *Front. Neuroendocrinol.* **2008**, *29*, 70−87.

(11) Adamantidis, A. R.; Zhang, F.; Aravanis, A. M.; Deisseroth, K.; de Lecea, L. Neural substrates of awakening probed with optogenetic control of hypocretin neurons. *Nature* **2007**, *450*, 420−424.

(12) de Lecea, L. Optogenetic control of hypocretin (orexin) neurons and arousal circuits. *Curr. Top. Behav. Neurosci.* **2015**, *25*, 367−378.

(13) Furlong, T. M.; Vianna, D. M. L.; Liu, L.; Carrive, P. Hypocretin/orexin contributes to the expression of some but not all forms of stress and arousal. *Eur. J. Neurosci.* **2009**, *30*, 1603−1614.

(14) Johnson, P. L.; Truitt, W.; Fitz, S. D.; Minick, P. E.; Dietrich, A.; Sanghani, S.; Träskman-Bendz, L.; Goddard, A. W.; Brundin, L.; Shekhar, A. A key role for orexin in panic anxiety. *Nat. Med.* **2010**, *16*, 111−115.

(15) Johnson, P. L.; Federici, L. M.; Fitz, S. D.; Renger, J. J.; Shireman, B.; Winrow, C. J.; Bonaventure, P.; Shekhar, A. Orexin 1 and 2 receptor involvement in co2 -induced panic-associated behavior and autonomic responses. *Depress. Anxiety* **2015**, *32*, 671−683.

(16) Bonaventure, P.; Yun, S.; Johnson, P. L.; Shekhar, A.; Fitz, S. D.; Shireman, B. T.; Lebold, T. P.; Nepomuceno, D.; Lord, B.; Wennerholm, M.; Shelton, J.; Carruthers, N.; Lovenberg, T.; Dugovic, C. A selective orexin-1 receptor antagonist attenuates stress-induced hyperarousal without hypnotic effects. *J. Pharmacol. Exp. Ther.* **2015**, *352*, 590−601.

(17) Kessler, B. A.; Stanley, E. M.; Frederick-Duus, D.; Fadel, J. Age-related loss of orexin/hypocretin neurons. *Neuroscience* **2011**, *178*, 82−88.

(18) Nixon, J. P.; Mavanji, V.; Butterick, T. A.; Billington, C. J.; Kotz, C. M.; Teske, J. A. Sleep disorders, obesity, and aging: The role of orexin. *Ageing Res. Rev.* **2015**, *20*, 63−73.

(19) Yang, L.; Zou, B.; Xiong, X.; Pascual, C.; Xie, J.; Malik, A.; Xie, J.; Sakurai, T.; Xie, X. Hypocretin/orexin neurons contribute to hippocampus-dependent social memory and synaptic plasticity in mice. *J. Neurosci.* **2013**, *33*, 5275−5284.
(20) Mavanji, V.; Butterick, T. A.; Duffy, C. M.; Nixon, J. P.; Billington, C. J.; Kotz, C. M. Orexin/hypocretin treatment restores hippocampal-dependent memory in orexin-deficient mice. *Neurobiol. Learn. Mem.* **2017**, *146*, 21−30.
(21) Mahoney, C. E.; Cogswell, A.; Koralnik, I. J.; Scammell, T. E. The neurobiological basis of narcolepsy. *Nat. Rev. Neurosci.* **2019**, *20*, 83−93.
(22) Nishino, S.; Ripley, B.; Overeem, S.; Lammers, G. J.; Mignot, E. Hypocretin (orexin) deficiency in human narcolepsy. *Lancet* **2000**, *355*, 39−40.
(23) Peyron, C.; Faraco, J.; Rogers, W.; Ripley, B.; Overeem, S.; Charnay, Y.; Nevsimalova, S.; Aldrich, M.; Reynolds, D.; Albin, R.; Li, R.; Hungs, M.; Pedrazzoli, M.; Padigaru, M.; Kucherlapati, M.; Fan, J.; Maki, R.; Lammers, G. J.; Bouras, C.; Kucherlapati, R.; Nishino, S.; Mignot, E. A mutation in a case of early onset narcolepsy and a generalized absence of hypocretin peptides in human narcoleptic brains. *Nat. Med.* **2000**, *6*, 991−997.
(24) Thannickal, T. C.; Moore, R. Y.; Nienhuis, R.; Ramanathan, L.; Gulyani, S.; Aldrich, M.; Cornford, M.; Siegel, J. M. Reduced number of hypocretin neurons in human narcolepsy. *Neuron* **2000**, *27*, 469−474.
(25) Mavanji, V.; Perez-Leighton, C. E.; Kotz, C. M.; Billington, C. J.; Parthasarathy, S.; Sinton, C. M.; Teske, J. A. Promotion of wakefulness and energy expenditure by orexin-a in the ventrolateral preoptic area. *Sleep* **2015**, *38*, 1361−1370.
(26) Tsujino, N.; Sakurai, T. Role of orexin in modulating arousal, feeding, and motivation. *Front. Behav. Neurosci.* **2013**, *7*, 28.
(27) Fadel, J. R.; Jolivalt, C. G.; Reagan, L. P. Food for thought: The role of appetitive peptides in age-related cognitive decline. *Ageing Res. Rev.* **2013**, *12*, 764−776.
(28) Davies, J.; Chen, J.; Pink, R.; Carter, D.; Saunders, N.; Sotiriadis, G.; Bai, B.; Pan, Y.; Howlett, D.; Payne, A.; Randeva, H.; Karteris, E. Orexin receptors exert a neuroprotective effect in alzheimer's disease (ad) via heterodimerization with gpr103. *Sci. Rep.* **2015**, *5*, 12584.
(29) Fronczek, R.; van Geest, S.; Frölich, M.; Overeem, S.; Roelandse, F. W. C.; Lammers, G. J.; Swaab, D. F. Hypocretin (orexin) loss in alzheimer's disease. *Neurobiol. Aging* **2012**, *33*, 1642−1650.
(30) Fronczek, R.; Overeem, S.; Lee, S. Y. Y.; Hegeman, I. M.; van Pelt, J.; van Duinen, S. G.; Lammers, G. J.; Swaab, D. F. Hypocretin (orexin) loss in parkinson's disease. *Brain* **2007**, *130*, 1577−1585.
(31) Thannickal, T. C.; Lai, Y.-Y.; Siegel, J. M. Hypocretin (orexin) cell loss in parkinson's disease. *Brain* **2007**, *130*, 1586−1595.
(32) Thannickal, T. C.; Lai, Y. Y.; Siegel, J. M. Hypocretin (orexin) and melanin concentrating hormone loss and the symptoms of parkinson's disease. *Brain* **2008**, *131*, No. e87.
(33) Chow, M.; Cao, M. The hypocretin/orexin system in sleep disorders: Preclinical insights and clinical progress. *Nat. Sci. Sleep* **2016**, *8*, 81−86.
(34) Mieda, M.; Sakurai, T. Orexin (hypocretin) receptor agonists and antagonists for treatment of sleep disorders. Rationale for development and current status. *CNS Drugs* **2013**, *27*, 83−90.
(35) Lebold, T. P.; Bonaventure, P.; Shireman, B. T. Selective orexin receptor antagonists. *Bioorg. Med. Chem. Lett.* **2013**, *23*, 4761−4769.
(36) Perrey, D. A.; Zhang, Y. Therapeutics development for addiction: Orexin-1 receptor antagonists. *Brain Res.* **2020**, *1731*, 145922.
(37) Andrews, S. P.; Aves, S. J.; Christopher, J. A.; Nonoo, R. Orexin receptor antagonists: Historical perspectives and future opportunities. *Curr. Top. Med. Chem.* **2016**, *16*, 3438−3469.
(38) Boss, C.; Roch, C. Orexin research: Patent news from 2016. *Expert Opin. Ther. Pat.* **2017**, *27*, 1123−1133.
(39) Roecker, A. J.; Cox, C. D.; Coleman, P. J. Orexin receptor antagonists: New therapeutic agents for the treatment of insomnia. *J. Med. Chem.* **2016**, *59*, 504−530.
(40) Boutrel, B.; Kenny, P. J.; Specio, S. E.; Martin-Fardon, R.; Markou, A.; Koob, G. F.; de Lecea, L. Role for hypocretin in mediating stress-induced reinstatement of cocaine-seeking behavior. *Proc. Natl. Acad. Sci. U.S.A.* **2005**, *102*, 19168−19173.
(41) James, M. H.; Mahler, S. V.; Moorman, D. E.; Aston-Jones, G. A decade of orexin/hypocretin and addiction: Where are we now? *Curr. Top. Behav. Neurosci.* **2017**, *33*, 247−281.
(42) Bonaventure, P.; Dugovic, C.; Shireman, B.; Preville, C.; Yun, S.; Lord, B.; Nepomuceno, D.; Wennerholm, M.; Lovenberg, T.; Carruthers, N.; Fitz, S. D.; Shekhar, A.; Johnson, P. L. Evaluation of jnj-54717793 a novel brain penetrant selective orexin 1 receptor antagonist in two rat models of panic attack provocation. *Front. Pharmacol.* **2017**, *8*, 357.
(43) Yangisawa, M. Small-molecule agonists for type-2 orexin receptor. U.S. Patent 20,100,150,840 A1, 2010.
(44) Turku, A.; Rinne, M. K.; Boije af Gennäs, G.; Xhaard, H.; Lindholm, D.; Kukkonen, J. P. Orexin receptor agonist yan 7874 is a weak agonist of orexin/hypocretin receptors and shows orexin receptor-independent cytotoxicity. *PLoS One* **2017**, *12*, No. e0178526.
(45) Nagahara, T.; Saitoh, T.; Kutsumura, N.; Irukayama-Tomobe, Y.; Ogawa, Y.; Kuroda, D.; Gouda, H.; Kumagai, H.; Fujii, H.; Yanagisawa, M.; Nagase, H. Design and synthesis of non-peptide, selective orexin receptor 2 agonists. *J. Med. Chem.* **2015**, *58*, 7931−7937.
(46) Irukayama-Tomobe, Y.; Ogawa, Y.; Tominaga, H.; Ishikawa, Y.; Hosokawa, N.; Ambai, S.; Kawabe, Y.; Uchida, S.; Nakajima, R.; Saitoh, T.; Kanda, T.; Vogt, K.; Sakurai, T.; Nagase, H.; Yanagisawa, M. Nonpeptide orexin type-2 receptor agonist ameliorates narcolepsy-cataplexy symptoms in mouse models. *Proc. Natl. Acad. Sci. U.S.A.* **2017**, *114*, 5731−5736.
(47) Toyama, S.; Shimoyama, N.; Tagaito, Y.; Nagase, H.; Saitoh, T.; Yanagisawa, M.; Shimoyama, M. Nonpeptide orexin-2 receptor agonist attenuates morphine-induced sedative effects in rats. *Anesthesiology* **2018**, *128*, 992−1003.
(48) Yukitake, H.; Fujimoto, T.; Ishikawa, T.; Suzuki, A.; Shimizu, Y.; Rikimaru, K.; Ito, M.; Suzuki, M.; Kimura, H. Tak-925, an orexin 2 receptor-selective agonist, shows robust wake-promoting effects in mice. *Pharmacol. Biochem. Behav.* **2019**, *187*, 172794.
(49) Bogen, S. L.; Clausen, D. J.; Guiadeen, D. G.; rudd, M. T.; Yang, D. 5-alkyl pyrrolidine orexin receptor agonists. U.S. Patent 20,200,255,403 A1, 2020.
(50) Hong, C.; Byrne, N. J.; Zamlynny, B.; Tummala, S.; Xiao, L.; Shipman, J. M.; Partridge, A. T.; Minnick, C.; Breslin, M. J.; Rudd, M. T.; Stachel, S. J.; Rada, V. L.; Kern, J. C.; Armacost, K. A.; Hollingsworth, S. A.; O'Brien, J. A.; Hall, D. L.; McDonald, T. P.; Strickland, C.; Brooun, A.; Soisson, S. M.; Hollenstein, K. Structures of active-state orexin receptor 2 rationalize peptide and small-molecule agonist recognition and receptor activation. *Nat. Commun.* **2021**, *12*, 815.
(51) Marcus, J. N.; Aschkenasi, C. J.; Lee, C. E.; Chemelli, R. M.; Saper, C. B.; Yanagisawa, M.; Elmquist, J. K. Differential expression of orexin receptors 1 and 2 in the rat brain. *J. Comp. Neurol.* **2001**, *435*, 6−25.
(52) Lu, J.; Bjorkum, A. A.; Xu, M.; Gaus, S. E.; Shiromani, P. J.; Saper, C. B. Selective activation of the extended ventrolateral preoptic nucleus during rapid eye movement sleep. *J. Neurosci.* **2002**, *22*, 4568−4576.
(53) Mieda, M.; Hasegawa, E.; Kisanuki, Y. Y.; Sinton, C. M.; Yanagisawa, M.; Sakurai, T. Differential roles of orexin receptor-1 and -2 in the regulation of non-rem and rem sleep. *J. Neurosci.* **2011**, *31*, 6518−6526.
(54) Willie, J. T.; Chemelli, R. M.; Sinton, C. M.; Tokita, S.; Williams, S. C.; Kisanuki, Y. Y.; Marcus, J. N.; Lee, C.; Elmquist, J. K.; Kohlmeier, K. A.; Leonard, C. S.; Richardson, J. A.; Hammer, R. E.; Yanagisawa, M. Distinct narcolepsy syndromes in orexin receptor-2

and orexin null mice: Molecular genetic dissection of non-rem and rem sleep regulatory processes. *Neuron* **2003**, *38*, 715−730.
(55) Chemelli, R. M.; Willie, J. T.; Sinton, C. M.; Elmquist, J. K.; Scammell, T.; Lee, C.; Richardson, J. A.; Williams, S. C.; Xiong, Y.; Kisanuki, Y.; Fitch, T. E.; Nakazato, M.; Hammer, R. E.; Saper, C. B.; Yanagisawa, M. Narcolepsy in orexin knockout mice: Molecular genetics of sleep regulation. *Cell* **1999**, *98*, 437−451.
(56) Willie, J. T.; Chemelli, R. M.; Sinton, C. M.; Yanagisawa, M. To eat or to sleep? Orexin in the regulation of feeding and wakefulness. *Annu. Rev. Neurosci.* **2001**, *24*, 429−458.
(57) Gotter, A. L.; Forman, M. S.; Harrell, C. M.; Stevens, J.; Svetnik, V.; Yee, K. L.; Li, X.; Roecker, A. J.; Fox, S. V.; Tannenbaum, P. L.; Garson, S. L.; Lepeleire, I. D.; Calder, N.; Rosen, L.; Struyk, A.; Coleman, P. J.; Herring, W. J.; Renger, J. J.; Winrow, C. J. Orexin 2 receptor antagonism is sufficient to promote nrem and rem sleep from mouse to man. *Sci. Rep.* **2016**, *6*, 27147.
(58) Winrow, C. J.; Gotter, A. L.; Cox, C. D.; Doran, S. M.; Tannenbaum, P. L.; Breslin, M. J.; Garson, S. L.; Fox, S. V.; Harrell, C. M.; Stevens, J.; Reiss, D. R.; Cui, D.; Coleman, P. J.; Renger, J. J. Promotion of sleep by suvorexant-a novel dual orexin receptor antagonist. *J. Neurogenet.* **2011**, *25*, 52−61.
(59) Morairty, S. R.; Revel, F. G.; Malherbe, P.; Moreau, J.-L.; Valladao, D.; Wettstein, J. G.; Kilduff, T. S.; Borroni, E. Dual hypocretin receptor antagonism is more effective for sleep promotion than antagonism of either receptor alone. *PLoS One* **2012**, *7*, No. e39131.
(60) German, N. A.; Decker, A. M.; Gilmour, B. P.; Thomas, B. F.; Zhang, Y. Truncated orexin peptides: Structure-activity relationship studies. *ACS Med. Chem. Lett.* **2013**, *4*, 1224−1227.
(61) Webb, B.; Sali, A. Protein structure modeling with modeller. *Methods Mol. Biol.* **2017**, *1654*, 39−54.
(62) Kolossváry, I.; Keseru, G. Hessian-free low-mode conformational search for large-scale protein loop optimization: Application to c-jun n-terminal kinase jnk3. *J. Comput. Chem.* **2001**, *22*, 21−30.
(63) Case, D. A.; Ben-Shalom, I. Y.; Brozell, S. R.; Cerutti, D. S.; Cheatham, T. E., III; Cruzeiro, V. W. D.; Darden, T. A.; Duke, R. E.; Ghoreishi, D.; Gilson, M. K.; Goetz, H. G. W.; Greene, D.; Harris, R.; Homeyer, N.; Izadi, S.; Kovalenko, A.; Kurtzman, T.; Lee, T. S.; LeGrand, S.; Li, P.; Lin, C.; Liu, J.; Luchko, T.; Luo, R.; Mermelstein, D. J.; Merz, K. M.; Miao, Y.; Monard, G.; Nguyen, C.; Nguyen, H.; Omelyan, I.; Onufriev, A.; Pan, F.; Qi, R.; Roe, D. R.; Roitberg, A.; Sagui, C.; Schott-Verdugo, S.; Shen, J.; Simmerling, C. L.; Smith, J.; Salomon-Ferrer, R.; Swails, J.; Walker, R. C.; Wang, J.; Wei, H.; Wolf, R. M.; Wu, X.; Xiao, L.; York, D. M.; Kollman, P. A. *Amber 2018*, 2018.
(64) Case, D. A.; Betz, R. M.; Cerutti, D. S.; Cheatham, T. E., III; Darden, T. A.; Duke, R. E.; Giese, T. J.; Gohlke, H.; Goetz, A. W.; Homeyer, N.; Izadi, S.; Janowski, P.; Kaus, J.; Kovalenko, A.; Lee, T. S.; LeGrand, S.; Li, P.; Lin, C.; Luchko, T.; Luo, R.; Madej, B.; Mermelstein, D.; Merz, K. M.; Monard, G.; Nguyen, H.; Nguyen, H. T.; Omelyan, I.; Onufriev, A.; Roe, D. R.; Roitberg, A.; Sagui, C.; Simmerling, C. L.; Botello-Smith, W. M.; Swails, J.; Walker, R. C.; Wang, J.; Wolf, R. M.; Wu, X.; Xiao, L.; Kollman, P. A. *AMBER 2016*; University of California: San Francisco, 2016.
(65) Dickson, C. J.; Madej, B. D.; Skjevik, Å. A.; Betz, R. M.; Teigen, K.; Gould, I. R.; Walker, R. C. Lipid14: The amber lipid force field. *J. Chem. Theory Comput.* **2014**, *10*, 865−879.
(66) Amato, G. S.; Manke, A.; Harris, D. L.; Wiethe, R. W.; Vasukuttan, V.; Snyder, R. W.; Lefever, T. W.; Cortes, R.; Zhang, Y.; Wang, S.; Runyon, S. P.; Maitra, R. Blocking alcoholic steatosis in mice with a peripherally restricted purine antagonist of the type 1 cannabinoid receptor. *J. Med. Chem.* **2018**, *61*, 4370−4385.
(67) Friesner, R. A.; Murphy, R. B.; Repasky, M. P.; Frye, L. L.; Greenwood, J. R.; Halgren, T. A.; Sanschagrin, P. C.; Mainz, D. T. Extra precision glide: Docking and scoring incorporating a model of hydrophobic enclosure for protein-ligand complexes. *J. Med. Chem.* **2006**, *49*, 6177−6196.
(68) Sherman, W.; Day, T.; Jacobson, M. P.; Friesner, R. A.; Farid, R. Novel procedure for modeling ligand/receptor induced fit effects. *J. Med. Chem.* **2006**, *49*, 534−553.
(69) Yin, J.; Mobarec, J. C.; Kolb, P.; Rosenbaum, D. M. Crystal structure of the human ox2 orexin receptor bound to the insomnia drug suvorexant. *Nature* **2015**, *519*, 247−250.
(70) Suno, R.; Kimura, K. T.; Nakane, T.; Yamashita, K.; Wang, J.; Fujiwara, T.; Yamanaka, Y.; Im, D.; Horita, S.; Tsujimoto, H.; Tawaramoto, M. S.; Hirokawa, T.; Nango, E.; Tono, K.; Kameshima, T.; Hatsui, T.; Joti, Y.; Yabashi, M.; Shimamoto, K.; Yamamoto, M.; Rosenbaum, D. M.; Iwata, S.; Shimamura, T.; Kobayashi, T. Crystal structures of human orexin 2 receptor bound to the subtype-selective antagonist empa. *Structure* **2018**, *26*, 7−19.
(71) Sakurai, T. The neural circuit of orexin (hypocretin): Maintaining sleep and wakefulness. *Nat. Rev. Neurosci.* **2007**, *8*, 171−181.
(72) Takenoshita, S.; Sakai, N.; Chiba, Y.; Matsumura, M.; Yamaguchi, M.; Nishino, S. An overview of hypocretin based therapy in narcolepsy. *Expert Opin. Invest. Drugs* **2018**, *27*, 389−406.
(73) Seigneur, E.; de Lecea, L. Hypocretin (orexin) replacement therapies. *Med. Drug Discovery* **2020**, *8*, 100070. In Press
(74) Sievers, F.; Higgins, D. G. Clustal omega for making accurate alignments of many protein sequences. *Protein Sci.* **2018**, *27*, 135−145.
(75) Wang, Q.; Canutescu, A. A.; Dunbrack, R. L., Jr. Scwrl and molide: Computer programs for side-chain conformation prediction and homology modeling. *Nat. Protoc.* **2008**, *3*, 1832−1847.
(76) Lee, T.-S.; Cerutti, D. S.; Mermelstein, D.; Lin, C.; LeGrand, S.; Giese, T. J.; Roitberg, A.; Case, D. A.; Walker, R. C.; York, D. M. Gpu-accelerated molecular dynamics and free energy methods in amber18: Performance enhancements and new features. *J. Chem. Inf. Model.* **2018**, *58*, 2043−2050.
(77) Watts, K. S.; Dalal, P.; Murphy, R. B.; Sherman, W.; Friesner, R. A.; Shelley, J. C. Confgen: A conformational search method for efficient generation of bioactive conformers. *J. Chem. Inf. Model.* **2010**, *50*, 534−546.
(78) Miller, E. B.; Murphy, R. B.; Sindhikara, D.; Borrelli, K. W.; Grisewood, M. J.; Ranalli, F.; Dixon, S. L.; Jerome, S.; Boyles, N. A.; Day, T.; Ghanakota, P.; Mondal, S.; Rafi, S. B.; Troast, D. M.; Abel, R.; Friesner, R. A. Reliable and accurate solution to the induced fit docking problem for protein-ligand binding. *J. Chem. Theory Comput.* **2021**, *17*, 2630−2639.


https://doi.org/10.1021/acs.jmedchem.1c00841
*J. Med. Chem.* 2021, 64, 8806−8825